MULTICOMPONENT COCRYSTALS AND SOLID SOLUTIONS BASED ON A TWO-POINT HYDROGEN BOND SYNTHON

by

Paul Ralph Emery

A Thesis

Submitted to the Faculty

of the

WORCESTER POLYTECHNIC INSTITUTE

in partial fulfillment of the requirements for the

Degree of Master of Science

in

Chemistry

January 15th, 2009

APPROVED:

Prof. Venkat R. Thalladi, Research Advisor

Signature _____ Date_____

Prof. Kristin N. Wobbe, Department Head

Signature _____ Date_____

Acknowledgements

I would like to express my gratitude to everyone who advised and assisted with this research while at WPI. Your time, opinions, and efforts are greatly appreciated.

To Professor Venkat R. Thalladi, my advisor. Thank you for your guidance, advice and friendship. The last four years of ideas, discussions, and research have been by far one of the greatest learning experiences I will ever know. Thank you so much.

I would like to thank Professor John C. MacDonald. Thank you again for all of your assistance and support while at WPI. From my first undergraduate course, to my MQP, and now this thesis, you have been a constant source of information and insight. Many thanks.

I would like to thank Dr. Richard Staples and Dr. Jingwei Huang at Harvard University for collecting single crystal X-ray data on dozens of crystals. This thesis would not be what it is without your help.

To my fellow group members Salimgerey Adilov, Jason Cox, and Marta Dabros. Thank you for your advice, patience, and camaraderie. My time spent at WPI, whether in the lab or otherwise, would never have been what it was without you each keeping me focused, honest, and smiling. You all have amazing futures to look forward to.

Finally, to the Faculty and Staff of the WPI Department of Chemistry and Biochemistry. Thank you all for your time, attention, and support. So many of you have influenced me as teachers, advisors, and fellow researchers, I can never thank you enough. God Bless.

Abbreviations and Acronyms

25AMP – 2-amino-5-methylpyridine

25ACP – 2-amino-5-chloropyridine

25ABP – 2-amino-5-bromopyridine

3-Cl-BA – 3-chlorobenzoic acid

3-CH_3-BA – 3-methylbenzoic acid (or: 3-toluic acid)

3-Br-BA – 3-bromobenzoic acid

4-I-BA – 4-iodobenzoic acid

4-Cl-BA – 4-chlorobenzoic acid

4-CH_3-BA – 4-methylbenzoic acid (or: 4-toluic acid)

4-Br-BA – 4-bromobenzoic acid

4-I-BA – 4-iodobenzoic acid

DABCO – 1,4-diazabicyclo[2.2.2]octane

L – liter

mL – milliliter

g – gram

mg – milligram

Abstract

Herein we describe a straight-forward and reproducible method for the preparation of homogeneous, multicomponent cocrystals and supramolecular solid solutions. We prepared these multicomponent materials based on small organic molecules that employ a two-point supramolecular hydrogen bond synthon. We report the creation and characterization of two, three, four, five, and seven component crystals containing a variety of 2-aminopyridines and monosubstituted benzoic acids. These systems exhibit the ability to accommodate multiple components in varying proportions while coordinating into an identical packing structure. The flexibility of the system to incorporate multiple components also gives rise to gradual modulation of physical properties.

Table of Contents

List of Figures

List of Tables

1. Introduction

Multicomponent solids date back to 4000 B.C. and the first ferrous alloys.[1] From ancient Egypt to the present, the study, design, and engineering of multicomponent materials have evolved from creating ornaments and small tools from the remains of iron-alloy meteorites to the forefront of modern technologies in the workplace, battlefield, and home. Metallurgy, material sciences, polymer chemistry, solid state chemistry, and crystal engineering are all disciplines that have developed from the pursuit of practical and innovative multicomponent solids. Our current work involves complexing two or more small organic molecules through specific intermolecular interactions into a single crystalline solid. Molecular association in single and multicomponent materials is best understood through the concepts of supramolecular chemistry.

1.1. Supramolecular Chemistry

Supramolecular chemistry is defined as "the chemistry beyond the molecule, bearing on the organized entries of higher complexity that result from the association of two or more chemical species held together by intermolecular forces."[2] Supermolecules, be they discrete or infinite, are formed by hydrogen bonds, π-π stacking, and other non-covalent interactions. In contrast, molecules are realized by making, destroying, and moving covalent bonds. Traditionally supramolecular chemistry is associated with molecular self-assembly in solution. Much of the earlier work was focused on binary assemblies involving an encompassing host and a fitting guest that exhibits chemical and geometrical complementarity. The connections between the enzyme-substrate recognition, coiling of double-stranded DNA with base-pair associations, and protein folding through hydrogen-bonding on the one hand,[3] and the emerging concept of anionic recognition by crown ethers and clatherates on the other hand,[4] are well recognized in the early days. Consequently, a large body of work has been carried out both to understand

the fundamentals of molecular recognition in its many facets and apply this knowledge in the design of new architectures to create materials and devices for practical use.[5] It is at this interface that the fields of supramolecular chemistry and crystal engineering have come together to usher the research in solid state chemistry in a new direction.[6]

1.2. Crystal Engineering

The origins of crystal engineering lie in the topochemical photoreactions carried out on cinnamic acids and their derivatives.[7] It is recognized in this early work that certain correlations can be established between crystal structures and molecular substitution patterns. For example, chloroaromatic groups tend to crystallize such that the aromatic rings are stacked within a distance of roughly 4 Å. This short separation enabled the photodimerization of olefinic double-bonds on cinnamic acids. Crystal engineering is defined as "the understanding of intermolecular interactions in the context of crystal packing and utilization of such understanding in the design of new crystal structures with designed physical and chemical properties."[6] Crystal engineering brought the principles of supramolecular chemistry to the solid state, and single and multicomponent crystals have become targets of supramolecular synthesis. In the context of current work, below we will briefly discuss the important terms and phrases used in this thesis.

1.3. Supramolecular Synthons

The fundamental building blocks of supramolecular chemistry are intermolecular interactions. These noncovalent interactions come in a number of forms, including hydrogen bonds, halogen bonds, π-stacking, and many more. *Supramolecular synthons* are defined as "structural units within supermolecules which can be formed and/or assembled by known or conceivable synthetic operations involving intermolecular interactions."[8] These synthons dictate molecular assembly throughout a crystalline material. We discuss supramolecular synthons in two categories. *Homosynthons* are

interactions between two identical hydrogen bonding moieties, and *heterosynthons* are interactions between two (or more) different yet complimentary acceptor-donor moieties. A number of supramolecular synthons are represented in Figure 1.

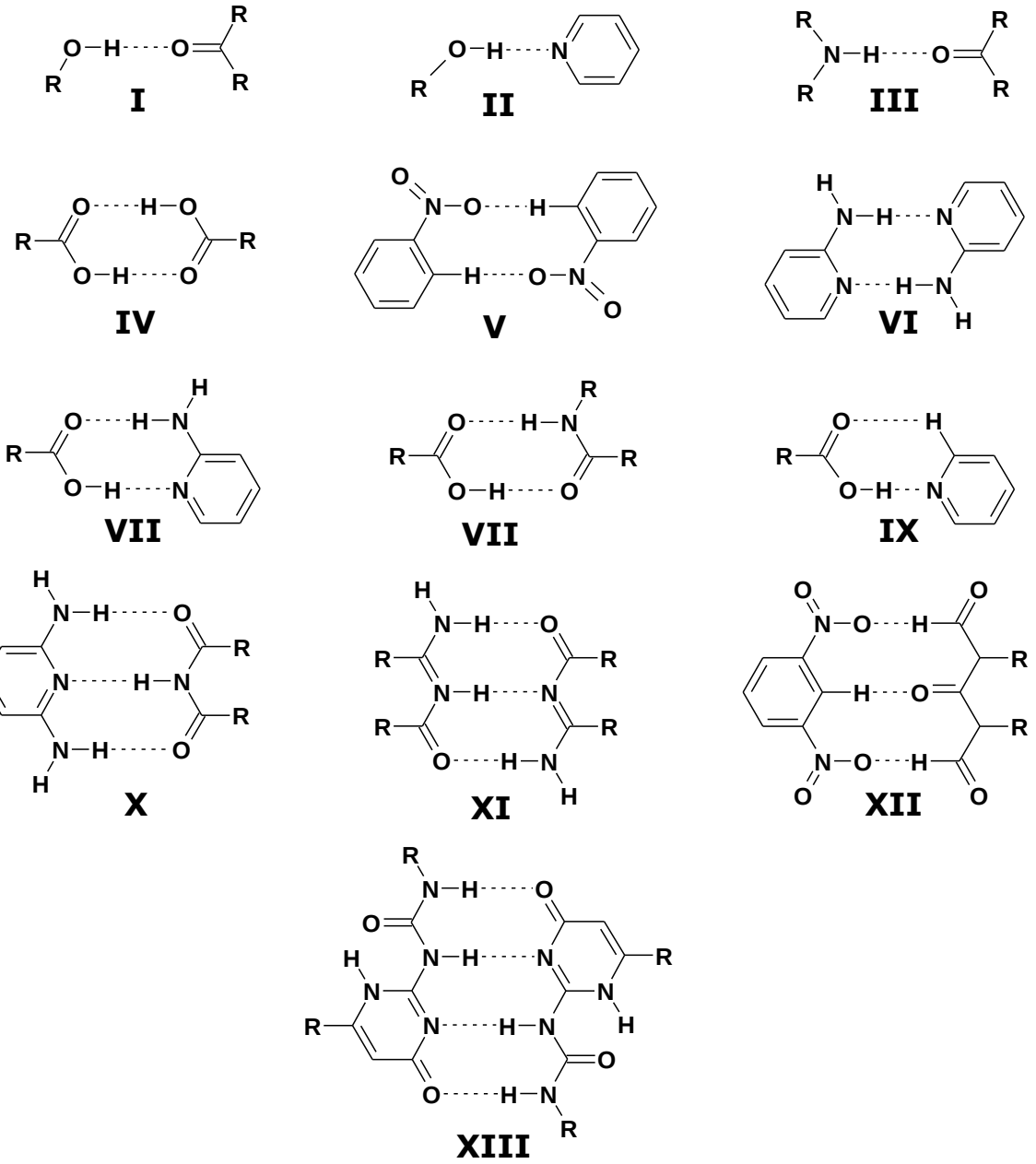

Figure 1. Examples of hydrogen bond synthons. Examples IV-VI, XI, and XIII are homosynthons.

Homosynthons formed by the carboxylic acid groups **(V)** can cause pure components to dimerize, creating a crystalline solid consisting of molecular pairs. Toluic acid, one of the moieties in our research, is an example that the carboxylic acid displays homosynthons in its crystal structure [9] The dimer generated by the association of two carboxylic acid groups is the repeating supermolecule within the crystal structure. One common example of heterosynthons is found between base pairings in a DNA strand.[10] In fact, heterosynthons such as the 2-aminopyridine-carboxylic acid synthon **(VII)** employed in our work may be preferable in crystal packing to possible homosynthons.[11] When these synthons are considered in the context of supramolecular chemistry, the associations between complimentary functional groups on different molecules result in multicomponent products. Nomenclature for these products depends on the nature of the association between different components. There is a current debate in literature on these very names.[12-15] In this thesis, we use the following nomenclature. A solute and solvent associate and crystallize to create a *solvate*, two components crystallize together through specific (and often predictable and discernible) synthons to generate a *cocrystal*, and multiple components associate within a single crystalline phase in nonstoichiometric ratios to produce a *solid solution*.[16]

1.4. Cocrystals

Molecular association by noncovalent interactions leads to liquidification and solidification. Depending on the range of the order within the resulting solid, from few hundred to few thousand molecules to several millions or more, the macroscopic solid is characterized as amorphous or crystalline. The same statements may be made for multicomponent systems. Within a multicomponent crystalline solid we find a supermolecule (an ensemble of two or more distinct molecules), not an individual molecule, as the smallest unit repeating regularly in three dimensions rather than a single molecule. Two distinct molecular species may form supramolecular assemblies in

various ratios (1:1, 2:1, 3:1, 3:2, etc.). As long as the supramolecular unit is consistent throughout the solid, the material is considered a cocrystal.[17] Figure 2 shows a schematic description of possible binary cocrystals of different stoichiometries.

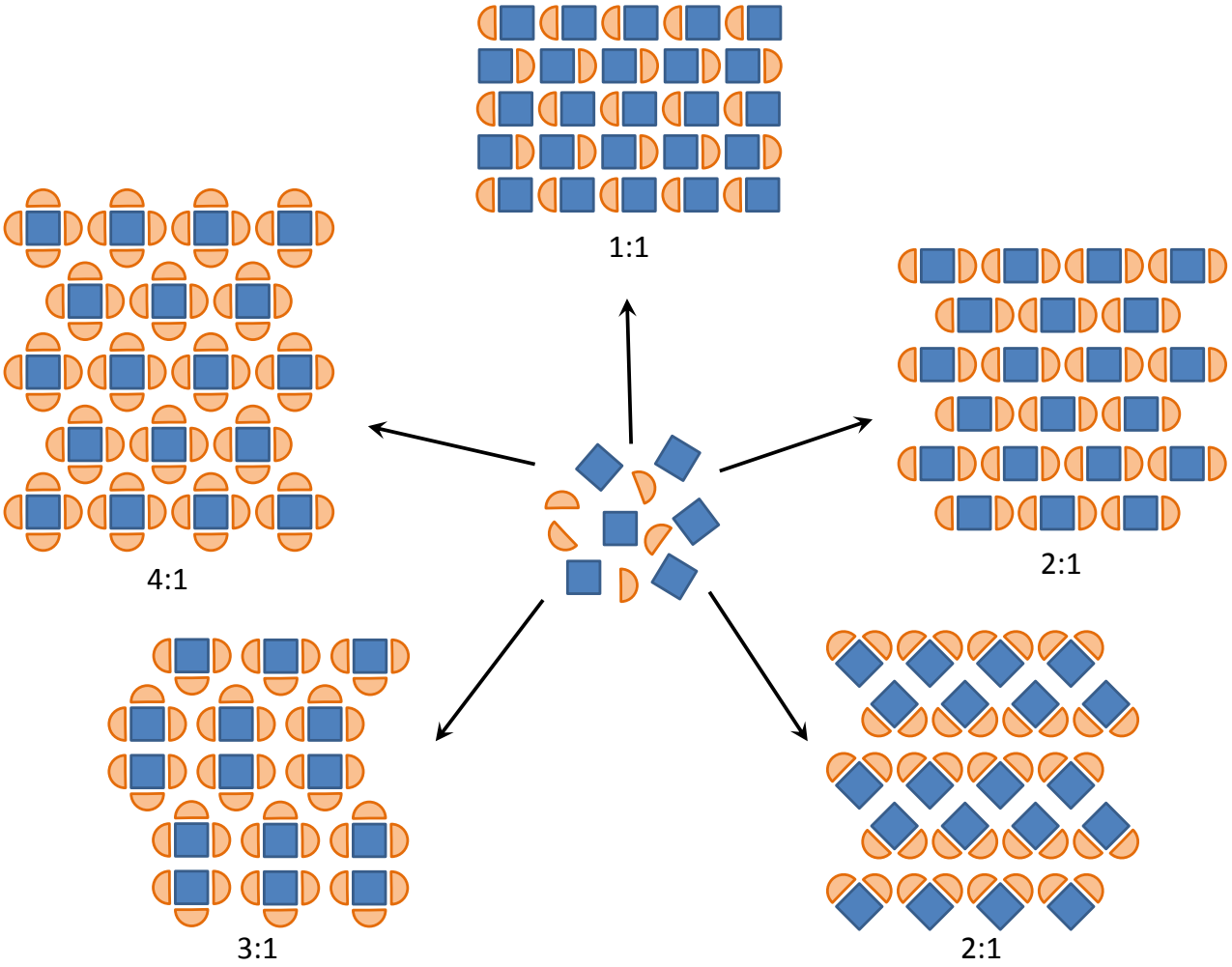

Figure 2. Examples of cocrystals with different stoichiometric ratios. All examples are binary; they contain only two distinct molecular entities.

1.5. Neutral versus Ionic Cocrystals

As discussed above, cocrystals can be obtained by complexing two or more molecules together by a variety of intermolecular interactions. For example, when a cocrystal is made by using π-stacking interactions, weak hydrogen bonds, or polarization induced halogen bonding, the resulting structure is most likely to be neutral. The two different components in such cocrystals associate by delocalization of electrons in the intermolecular space, but complete charge transfer does not occur. The two components are, for all practical purposes, charge neutral. Such cocrystals are considered in this work as *neutral cocrystals*.

Conversely, there are cocrystals that employ complete transfer of electrons or protons to induce charge assisted associations between moieties. In the case of strong hydrogen bonded synthons, the basic species (acceptor) may abstract the proton from the acidic species (donor) forming a charge-assisted hydrogen bond. This process results in the two species exchanging roles; the hydrogen donating species is deprotonated and becomes the hydrogen accepting species. In the context of our work these systems will be considered *ionic cocrystals*.[18, 19]

Carboxylic acid–pyridine supramolecular synthons vary depending on the relative acidic and basic properties of each species.[20] Cases in which the carboxylic acid species is highly acidic or the pyridine species is highly basic can result in the proton migrating to the pyridine, thus a charge-assisted carboxylate-pyridinium synthon is employed rather than the neutral analog. The neutral and charge-assisted synthons that can be formed between the carboxylic acid and pyridine moieties are shown in Figure 3.

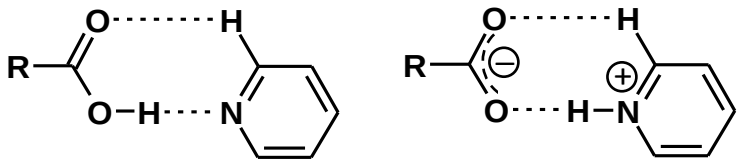

Figure 3. Neutral versus charge-assisted hydrogen bonding that can lead to neutral and ionic cocrystals.

1.6. Polymorphism

Polymorphism in molecular compounds is analogous to allotropy in pure elemental materials, wherein a chemical element has the ability to arrange in different solid state structures. The most notable example of allotropy is that of two carbon arrangements in the solid state, graphite and diamond. The graphite structure is composed of ring-based, 2D sheets stacked upon one another to form a lattice whereas the diamond is the result of the carbon atoms forming a covalent matrix in all three dimensions. This packing variation amounts to incredible differences in properties of these two allotropes; graphite is a gray, soft, brittle material whereas diamond is dense and one of the hardest naturally occurring material on earth. These differences are exploited for practical uses. For example, lead in pencils has been replaced with graphite, which is easily sharpened and far less toxic while diamonds are used in abrasives and jewelry.

Polymorphism can be considered allotropy of molecular species. All of the same facts apply to the arrangement of molecules as they do to elements: different packing structures result in different properties. The only measureable difference is the manner in which the units are associated with one another.[21] Elements are bonded in both covalent and noncovalent fashions whereas crystal packing for molecules is based on noncovalent bonding. Variations in physical properties between polymorphs are especially important for pharmaceutical products.[22, 23] Characteristics such as stability, solubility, and bioavailability define the scope of unique dosage forms and portray have major

ramifications for both the patient and the corporations developing and marketing pharmaceutical drugs.

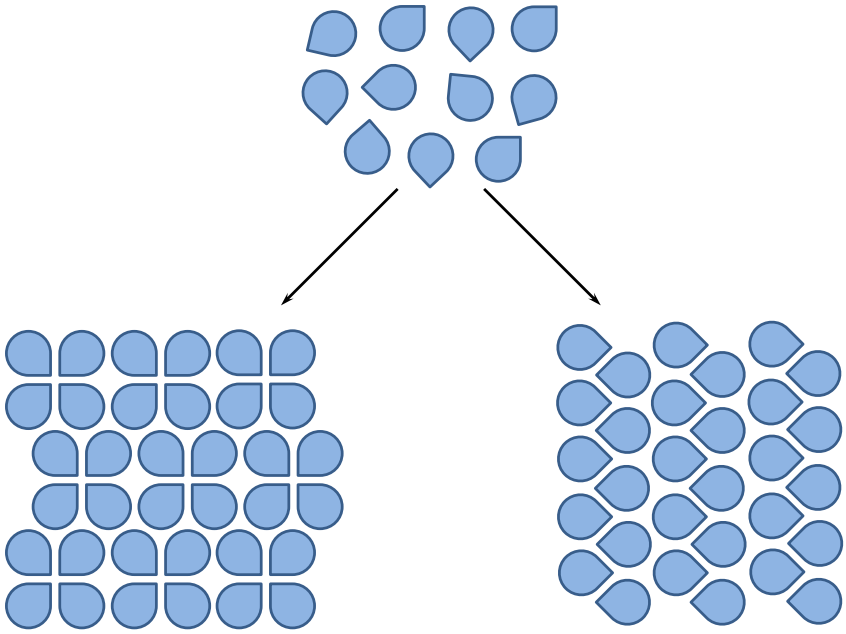

Figure 4. Schematic illustration of polymorphs of a single molecular compound.

Polymorphism, by its very definition, is not restricted to single component materials; cocrystals and solid solutions can also be polymorphic.[24] Figure 5 shows an example of how a binary 1:2 cocrystal may have multiple polymorphs.

This study involves the preparation of several cocrystals and solid solutions, and it is imperative to explore as many possible polymorphs that may occur in these systems, and to ensure that the structures reported based on single crystal data are representative of the bulk samples obtained in the crystallization experiments. We use powder X-ray diffraction (PXRD) as the primary means to correlate the diffraction patterns of bulk samples with the calculated patterns obtained from single crystal structures.

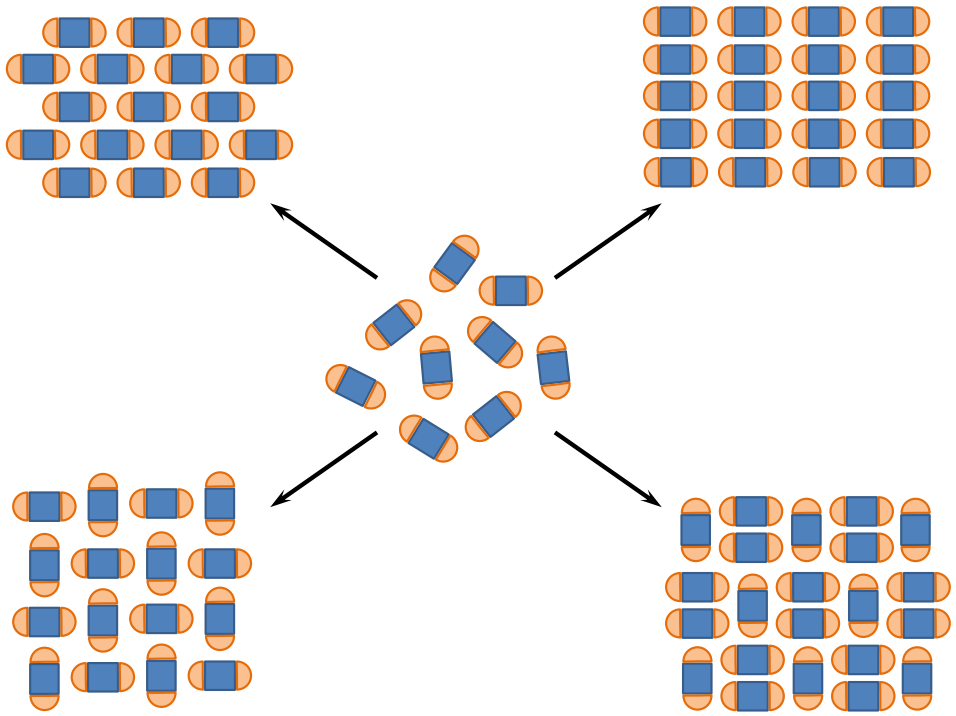

Figure 5. Schematic illustration of some polymorphs of a binary 1:2 cocrystal. Note the difference in the type of polymorphism shown here and in Figure 1.

1.7. Molecular Solid Solutions

As a pure material crystallizes, individual molecules associate with one another, packing in an arrangement that minimizes the overall energy within the system. The final orientation of the crystal results in each of the molecules packed closely together, with weak interactions between any single molecule and the molecules surrounding it. Interestingly, if an analogous material (or multiple analogous materials) is (are) introduced during crystallization (preferably that would crystallize in a similar solid state structure when alone), these multiple species may begin to crystallize into one single lattice. Put simply, the materials are so alike that no distinction is made between them, and readily replace one another within the crystal, producing a homogeneous solid solution. The relative quantities of each individual moiety may vary throughout the solid, but the overall structure of the crystal remains unchanged. In terms of our work we

consider these systems *molecular solid solutions*. These systems contain multiple molecules within a single lattice with localized domains of varying concentration.

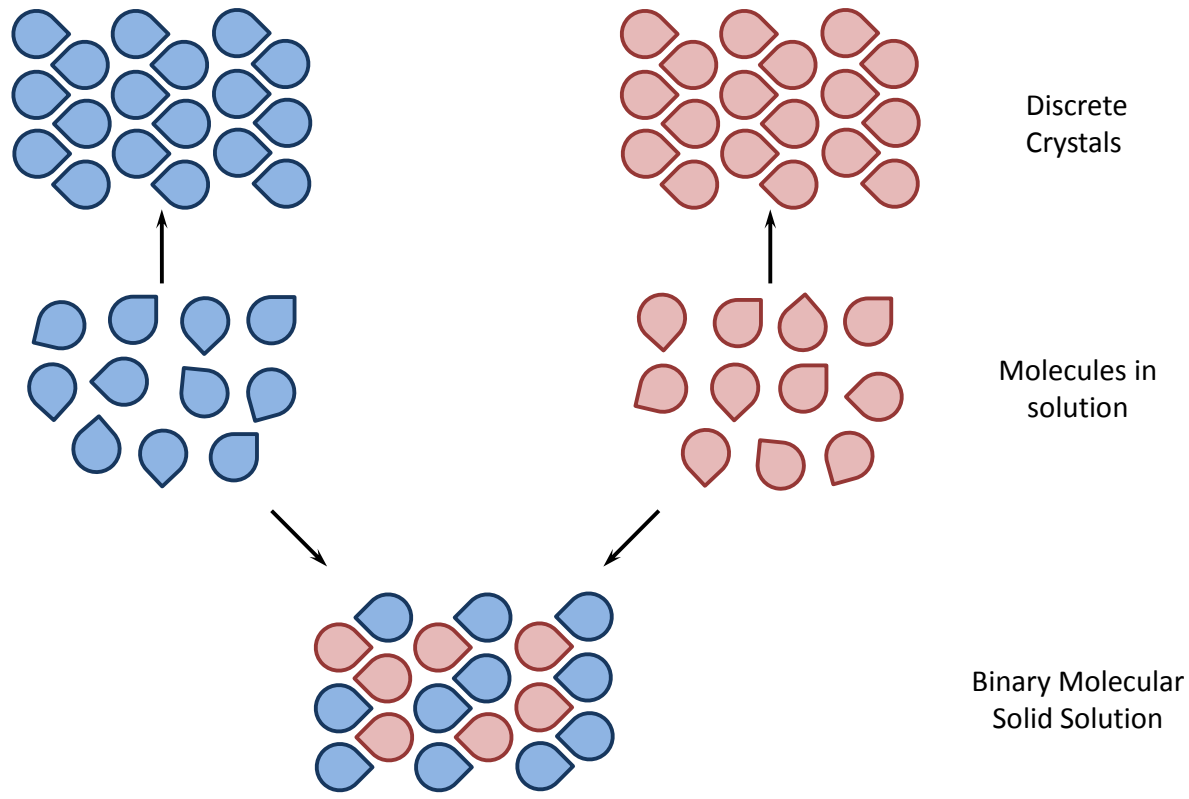

Figure 6. Schematic representation of a molecular solid solution. In this model, two molecules of similar size and comparable crystal packing crystallize together, readily replacing one another in the lattice.

1.8. Supramolecular Solid Solutions

In this work we combine the approaches of cocrystals and molecular solid solutions to prepare a new class of materials called *supramolecular solid solutions*. These materials are designed by incorporating the specificity of supramolecular synthons and the analogous geometry concepts vital to molecular solid solutions to combine multiple, different molecular species into one homogenous crystal.

The design of supramolecular solid solutions begins with the selection of a suitable supramolecular synthon to be used by multiple acceptor and donator moieties. However, in the case of supramolecular solid solutions, the acceptors must be structurally analogous to one another, the same for the donors. This design strategy provides the system with the ability to generate supermolecules of any acceptor-donor pair that would have functionally analogous structures. Figure 7 provides one example of a supramolecular solid solution employing one acceptor and two analogous donor moieties.

In the case of our solid solutions, we are no longer using analogous molecular moieties as our repeating unit. Instead, structurally analogous supermolecules, comprised of different acceptor-donor combinations, crystallize into a homogeneous matrix. This allows us to employ a much more diverse population of moieties in the pursuit of multicomponent systems. Rather than being bound to one group of structurally analogous molecules combining to form a molecular solid solution, we may instead design and create systems based entirely on supramolecular units.

The principal advantage of solid solutions is that their properties can be modulated by the graduate modification of the relative ratio of the components. For example, solid solutions of insulin and a lipophilically modified insulin derivative show superior *in-vivo* therapeutic properties.[25]

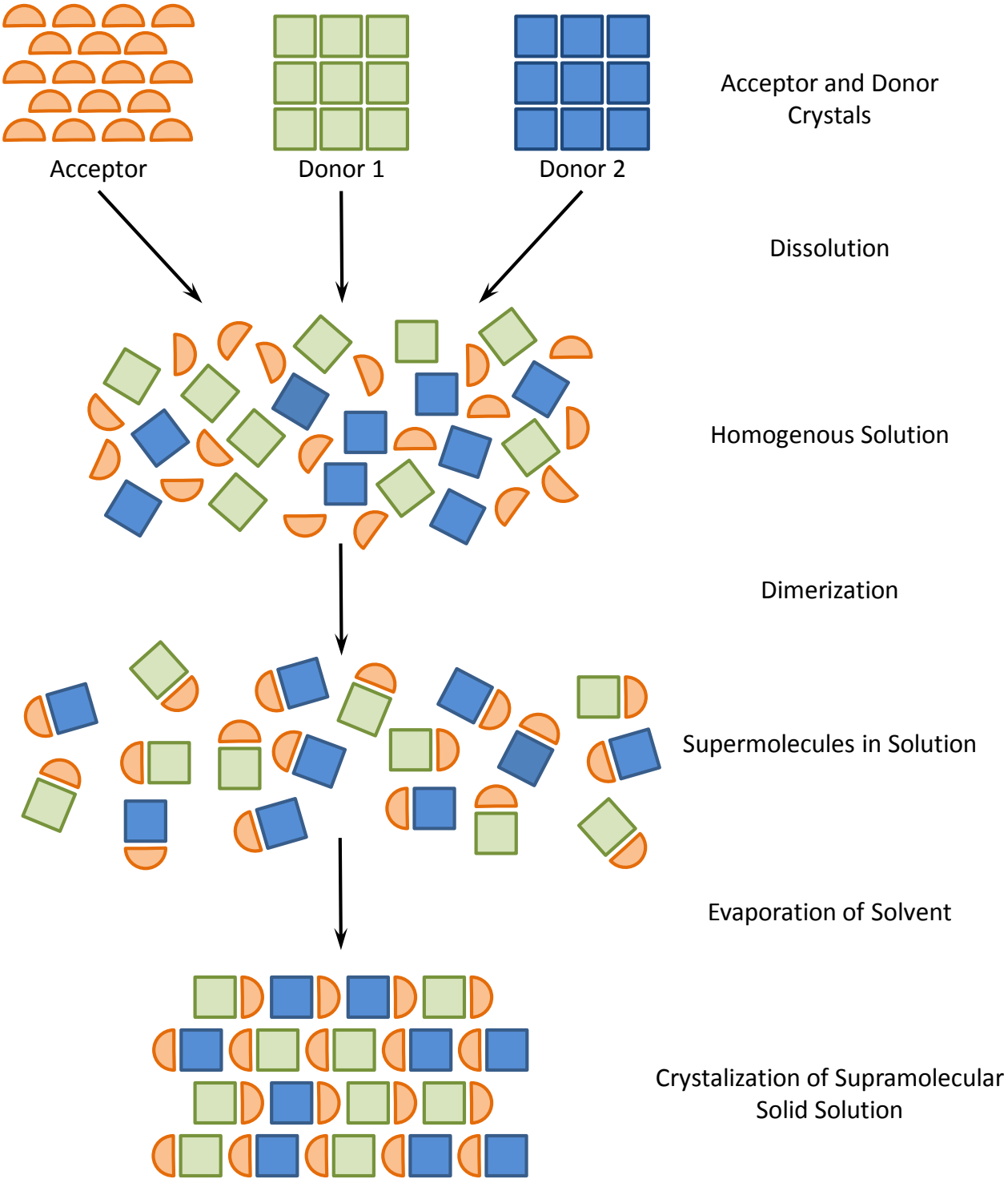

Figure 7. Schematic illustration of a supramolecular solid solution. Two similar donors and one acceptor are dissolved in solution. Acceptors join to both donor moieties to form two distinct supermolecules of similar size and shape while in solution. The two structurally analogous supermolecules pack into one homogeneous crystalline solid as solvent evaporates.

1.9. Prior Work on Supramolecular Solid Solutions

Previously we designed and created cocrystals and multicomponent supramolecular solid solutions using a single-point supramolecular synthon between a *bis*-acceptor moiety and multiple analogous donors.[26] 1,4-diazabicyclo[2.2.2]octane (DABCO, dual-acceptor) was dissolved in benzene with multiple *para*-substituted phenols (donors) and left to crystallize via slow evaporation at ambient laboratory conditions. Characterization of the crystalline products showed that they are indeed cocrystals and supramolecular solid solutions of DABCO with one or more phenols employing the trimolecular assembly shown in Figure 8.

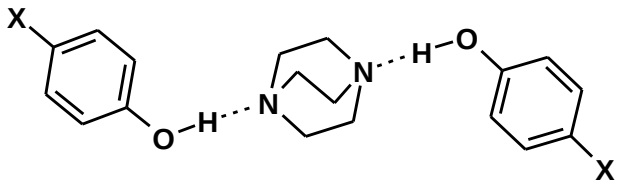

ClCl:	X = Cl		binary cocrystals
MeMe:	X = CH_3		
BrBr:	X = Br		
ClMe:	X = nCl + (1-n)CH_3	(0 > n > 1)	ternary solid solutions
ClBr:	X = nCl + (1-n)Br	(0 > n > 1)	
MeBr:	X = nCH_3 + (1-n)Br	(0 > n > 1)	
ClMeBr:	X = 1/3 Cl + 1/3 CH_3 + 1/3 Br		quaternary solid solution

Figure 8. Trimolecular DABCO-phenol assembly. Multiple *para*-substituted phenols were crystallized with DABCO employing a single-point supramolecular synthon.

These studies concluded with the successful creation of multiple cocrystals and supramolecular solid solutions varying from two- to four-components.

We reviewed the strengths and weaknesses of this study looking for ways to improve upon it. Primarily, there is inherent weakness in the single-point synthon

employed. The phenols are free to rotate 360° degrees about the O-H bond used in the supramolecular synthon. This conformational freedom in solution may inhibit the supramolecular structure from crystallizing with other assemblies and generate multiple packing arrangements (polymorphs) since the trimolecular assembly may take many forms. This activity is shown when comparing the crystal structures of the **ClCl** and **BrBr** cocrystals: the two systems crystallize in different packing arrangements. A two-point synthon may assist in removing this variability in cocrystal systems as well as increase the possibility for a greater number of components to coexist in a supramolecular solid solution.

Secondly, the donor was the only moiety that varied throughout this study of DABCO and phenols. The structure of DABCO was too specific to allow for substitutions to be made easily without affecting the size and shape of the molecule. In order to truly test the diversity of our supramolecular synthon and the assembly as a whole, the acceptor moiety should be varied by numerous substitutions as well.

2. Methodology

We have selected the aminopyridine-carboxylic acid heterosynthon (Figure 9) for creating multicomponent solids in this study. This synthon is selected due in part to the breadth of possibilities for acceptable moieties capable of utilizing this specific recognition motif, ranging from small organic molecules to pharmaceutical drugs, but also due to some recent literature showing the effectiveness of the synthon. Recently, this particular heterosynthon has been shown to dominate when both the carboxylic acid and aminopyridine functional groups are present, besting the two available homosynthons (carboxylic acid dimer, aminopyridine dimer) more often than not.[6]

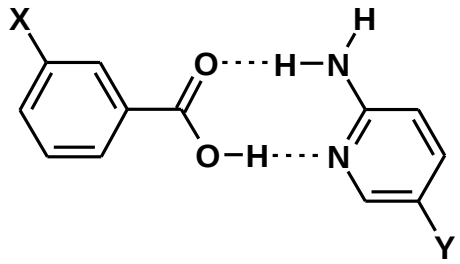

Figure 9. Aminopyridine-carboxylic acid heterosynthon. The benzoic acid moiety is shown with a *meta*-substituent. The 2-aminopyridine moiety is shown with a substituent at the 5-position.

The second step in our design is the selection of the components. The first set of components consists of three 5-substituted 2-aminopyradines: 2-amino-5-chloropyridine (25ACP), 2-amino-5-methylpyridine (25AMP), and 2-amino-5-bromopyridine (25ABP). See figure 10. These aminopyridines are readily available from commercial sources: they are all solids at room temperature.

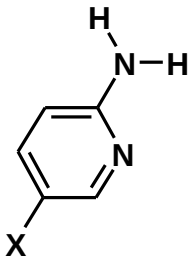

Figure 10. 2-amino-5-X-pyridine. X = Cl, CH_3, or Br.

The second component of our selected heterosynthon is the carboxylic acid group. For the purpose of these studies benzoic acids provided the appropriate carboxylic acid functional group. It is also worth mentioning that benzoic acid is listed among the FDA's GRAS (Generally Regarded As Safe) as a food preservative,[27] although for the purpose of this work only substituted benzoic acids were employed. Monosubstituted chloro-, methyl-, bromo-, and iodobenzoic acids were used in this study, with substitutions at both

the *meta*- and *para*- positions of the benzene ring, shown in Figure 11. These pyridines and benzoic acids, when mixed in solution, combine to form our selected synthon.

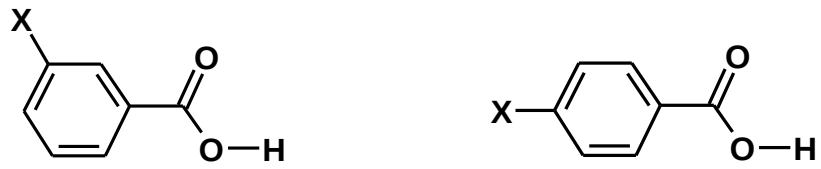

Figure 11. Benzoic acids substituted at the 3- and 4- positions with X groups. X = Cl, CH_3, Br, or I.

The selection of this two-point synthon improves upon our DABCO studies. As we noted previously, the single hydrogen bond synthon allowed the phenol groups to rotate freely about the O-H bond. The aminopyridine-carboxylic acid supramolecular synthon removes the ability for either moiety to rotate. Concurrently the two-point synthon can align the two moieties into a rigid, coplanar configuration. We expect that the minimization of conformational freedom in the dimeric assembly reduces the possibility of forming potentially different crystal structures. This two-point synthon also provides stronger association between the two moieties than the previously applied single-point supramolecular synthon, minimizing the free energy within the system, resulting in a higher affinity for cocrystallization. These are all ways that this supramolecular synthon selection may improve upon the previously selected single-point synthon.

Crystallized products were characterized using differential scanning calorimetry (DSC), Fourier transform infrared spectroscopy (FTIR), proton nuclear magnetic resonance spectroscopy(^{1}H-NMR), powder X-ray diffraction (PXRD), and single crystal X-ray diffraction (SXRD) methods.

2.1. Cocrystals

Experiments began with equimolar pyridine and acid mixtures dissolved in suitable solvents. Crystallization solutions were agitated by stirring or sonication or both and warmed to accelerate dissolution. The solutions were cooled to room temperature, covered with perforated aluminum foil or Parafilm, and left to evaporate under ambient laboratory conditions. Each substituted benzoic acid was combined with 25AMP in a 1:1 stoichiometric ratio to yield eight possible combinations, shown in Table 1.

Table 1. Possible binary (1:1) cocrystal experiments. Benzoic acids are referred by their substituents. For example, 3-Br refers to 3-bromobenzoic acid. In the text the acids are referred in the format 3-Br-BA.

***meta*-substituted acid combinations**	***para*-substituted acid combinations**
25AMP : 3-Cl	25AMP : 4-Cl
25AMP : 3-CH3	25AMP : 4-CH3
25AMP : 3-Br	25AMP : 4-Br
25AMP : 3-I	25AMP : 4-I

The first crystallizations were prepared in 10 mL scintillation glass vials with a total mass of less than 60 mg. As successful crystallizations produced harvestable crystals, experiments were repeated at larger scales. The last iterations of the cocrystal experiments were conducted in 25 mL Erlenmeyer flasks with a total mass greater than 200 mg. Data collected on individual crystallization experiments was compared directly to literature values for any previously identified cocrystals, as well as data collected from the characterization of raw materials used in each experiment, whether from literature or in-house characterization. Analysis of this data was also important in directing further research.

2.2. Ternary Solid Solutions

2.2.1. Equimolar Acid Experiments

Crystallizations of three component systems at 2:1:1 ratios of 25AMP to two benzoic acids marked the second tier of experimentation. All possible combinations were attempted without mixing *meta*- and *para*-substituted benzoic acids. Thus, all of the 3-X-benzoic acid combinations were attempted, then the 4-X-benzoic acid combinations. Table 2 shows all possible combinations of acids with 25AMP segregating the acids by their position of substitution.

Table 2. Possible ternary (2:1:1) solid solutions without mixing *meta*- and *para*-substituted benzoic acids.

***meta*-substituted acid combinations**	***para*-substituted acid combinations**
25AMP : 3-Cl : 3-CH3	25AMP : 4-Cl : 4-CH3
25AMP : 3-Cl : 3-Br	25AMP : 4-Cl : 4-Br
25AMP : 3-Cl : 3-I	25AMP : 4-Cl : 4-I
25AMP : 3-CH3 : 3-Br	25AMP : 4-CH3 : 4-Br
25AMP : 3-CH3 : 3-I	25AMP : 4-CH3 : 4-I
25AMP : 3-Br : 3-I	25AMP : 4-Br : 4-I

2.2.2. Variable Acid Ratio Experiments

Once the segregated experiments had concluded, two ternary systems were selected for further study at a larger scale. Relying on preliminary cocrystallization experiments, one mixed-position system and one segregated system were crystallized at varying stoichiometries. These two systems were selected based on two criteria: the initial cocrystal experiment yielded large, homogenous crystals and the single crystal X-ray diffraction data returned a similar packing structure for both the meta- and para- cocrystal

experiments. Two series of experiments that were developed based on this data are listed in Table 3.

Table 3. Variable molar ratio ternary solid solution studies.

Variable molar ratio ternary solid solution studies
25AMP : 3-Cl: 3-CH3
25AMP : 3-CH3 : 4-CH3

These studies would involve crystallizing moieties at 10% stoichiometric increments, beginning with 100% acid A to 0% acid B, then 90% acid A to 10% acid B, 80% A to 20% B, etc., completing each series with a crystallization at 0% acid A to 100% acid B. Thus, each series would be bracketed by large scale cocrystals.

2.3. Quaternary Solid Solutions

Four-component systems occupy the fourth tier of experimentation in our work. Experiments mixing three like-substituted acids with 25AMP in a 3:1:1:1 ratio results in systems with increasing numbers of components, but fewer possible combinations. Table 4 shows the eight possible experiments while continuing to keep substitution positions constant.

Table 4. Possible quaternary (3:1:1:1) solid solutions without mixing *meta*- and *para*-substituted benzoic acids.

***meta*-substituted acid combinations**	***para*-substituted acid combinations**
25AMP : 3-Cl : 3-CH3 : 3-Br	25AMP : 4-Cl : 4-CH3 : 4-Br
25AMP : 3-Cl : 3-CH3 : 3-I	25AMP : 4-Cl : 4-CH3 : 4-I
25AMP : 3-Cl : 3-Br : 3-I	25AMP : 4-Cl : 4-Br : 4-I
25AMP : 3-CH3 : 3-Br: 3-I	25AMP : 4-CH3 : 4-Br: 4-I

2.4. Quinary Solid Solutions

When all substitution-segregated acids are mixed with 25AMP, only two possible combinations are available. These experiments were conducted at 4:1:1:1:1 ratios, and were designed to produce five-component solid solution crystals. Once again, only acids of like-substitution position were mixed.

Table 5. Possible quinary (4:1:1:1:1) solid solutions without mixing *meta*- and *para*-substituted benzoic acids.

***meta*-substituted acid combination**	***para*-substituted acid combination**
25AMP : 3-Cl : 3-CH3 : 3-Br : 3-I	25AMP : 4-Cl : 4-CH3 : 4-Br :4-I

2.5. Septary (Seven-Component) Solid Solutions

Now that all possible substitution-segregated benzoic acid experiments have been outlined with 25AMP, two experiments were outlined involving multiple aminopyridines. Like the quinary solid solution experiments explained above, all four like-substituted benzoic acids are employed. However, rather than being combined solely with 25AMP, both 25ACP and 25ABP are also added. The two combinations have seven unique moieties mixed in a 4:4:4:3:3:3:3 fashion, with a total mass of nearly 100 mg of raw materials.

Table 6. Possible septary (4:4:4:3:3:3:3) solid solutions without mixing *meta*- and *para*-substituted benzoic acids.

***meta*-substituted acid combination**	***para*-substituted acid combination**
25ACP : 25AMP : 25ABP : 3-Cl : 3-CH3 : 3-Br : 3-I	25ACP : 25AMP : 25ABP : 4-Cl : 4-CH3 : 4-Br :4-I

3. Results and Discussion

In order to confirm the presence of multicomponent solids, characterization of all raw materials was completed from both literature data and in-house methods. Once cocrystallization experiments had been completed they were characterized by the same methods as the raw material counterparts and compared directly. In the case of supramolecular solid solutions characterization data would be compared not only to raw materials, but to any cocrystals or solid solution possibilities therein (i.e., a solid solution of 25AMP, 3-Cl-BA, 3-CH_3-BA, and 3-Br-BA would be compared to all raw materials, all possible cocrystals, and the 25AMP/3-Cl/3CH_3, 25AMP/3-Cl/3-Br, and 25AMP/3-CH_3/3-Br solid solutions).

3.1. Fourier Transform Infrared Spectroscopy (FTIR)

FTIR spectra of raw materials were compared to literature data while cocrystallization products were compared to data from respective raw materials. Gross spectral changes were observed in the intensity and position of absorption peaks consistent with changes in characteristic bond environments. Spectra were obtained at ambient laboratory conditions from 4000-600 wavenumbers (cm^{-1}). Here we use the 25AMP/3-Cl-BA cocrystal as an example. Figure 12 shows the FTIR spectra of the cocrystal and the corresponding individual components.

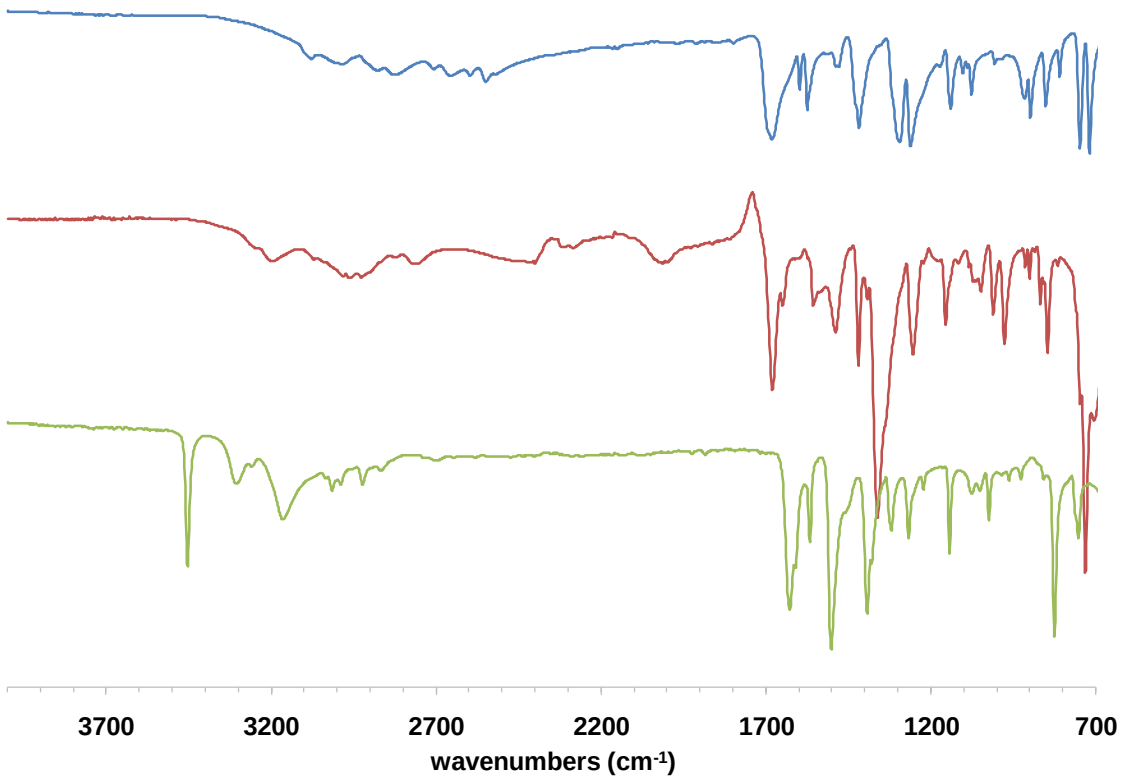

Figure 12. FTIR spectra of the 3-chlorobenzoic acid, 25AMP/3-Cl-BA (1:1) cocrystal, and 2-amino-5-methylpyridine (listed from top to bottom). In this and other FTIR spectra in this thesis, the y-axis represents % transmittance.

Raw material spectra are comparable to known literature spectra. Also note that all the spectra are unique; the expected cocrystal spectra is not similar to the spectra of the components. Specific observations in FTIR spectra will be discussed in greater detail later.

3.2. Differential Scanning Calorimetry (DSC)

Raw materials and harvested single crystals were analyzed by differential scanning calorimetry. Raw materials and expected cocrystals were compared to available literature values and analytical data. Samples were heated in the range of 25-300°C, ramped at 10°/min, in sealed aluminum pans. Figure 13 shows the thermal analysis of 25AMP/3-Cl-BA 1:1 cocrystal alongside the DSC data from its respective raw materials. The

prospective cocrystal continues to exhibit behavior different from the pyridine and benzoic acid components.

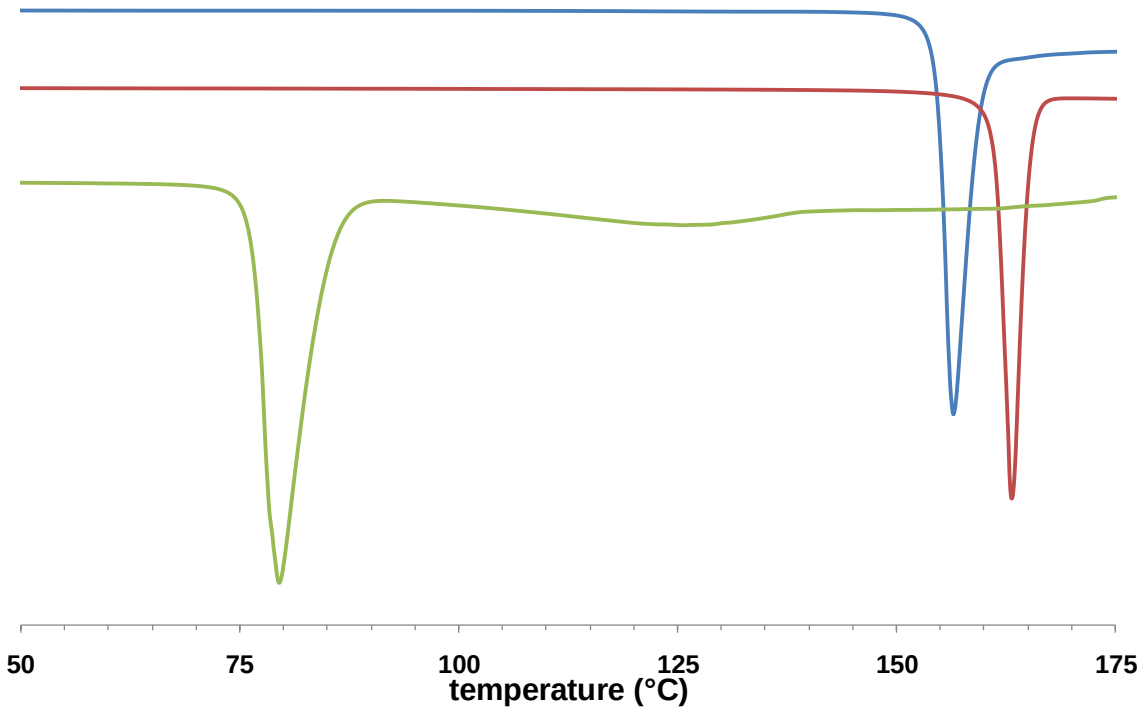

Figure 13. DSC thermograms of 3-chlorobenzoic acid (blue), 2-amino-5-methylpyridine (green), and the associated 1:1 cocrystal (red). In this and other DSC thermograms in this thesis, the y-axis represents % heat flow.

3.3. Powder X-Ray Diffraction (PXRD)

Powder X-ray data were collected on a Bruker AXS D8 Focus diffractometer using Cu-Kα radiation. The instrument was equipped with a vertical goniometer and a scintillation counter as a detector and applied Bragg-Brentano geometry for data collection. Samples were finely ground using a mortar and pestle and transferred to a glass sample holder that had loading dimensions 1.6 cm × 2 cm. The data were collected in the 2Θ range 5-50° (step size = 0.05°) and at a scan rate of 2° per minute. Figure S10 shows the diffraction patterns of binary cocrystals and ternary solid solutions; it is similar to Figure 3 except that the data were shown from 5-35° in 2Θ. Figure 14 shows the

PXRD patterns of 3-chlorobenzoic acid, 2-amino-5-methylpyridine, and the respective cocrystal.

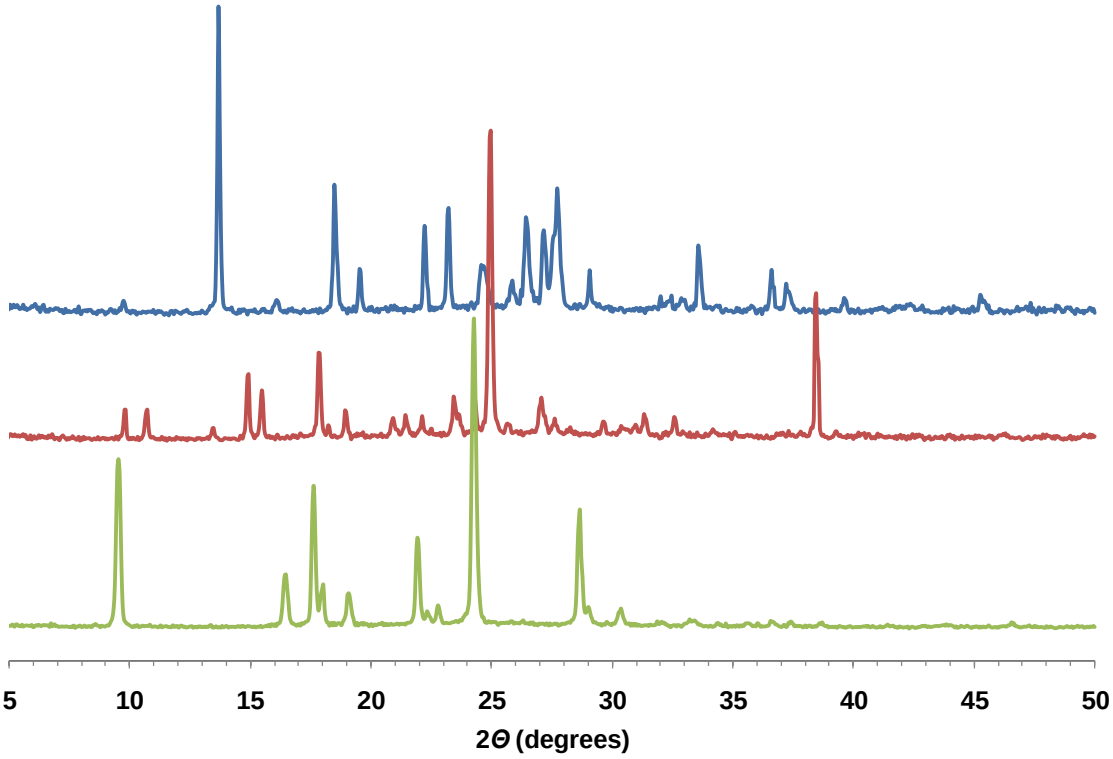

Figure 14: PXRD patterns of 25AMP (green), 3-Cl-BA (blue), and the respective 1:1 cocrystal (red). In this and other PXRD patterns in this thesis, the y-axis represents relative intensity.

3.4. Single Crystal X-Ray Diffraction (SXRD)

SXRD studies were performed on the majority of cocrystallization products. Crystals suitable for diffraction were selected under a microscope and mounted on a glass fiber using a small amount of paratone oil. X-ray data was collected using a Bruker SMART diffractometer equipped with a CCD detector and an Oxford Cryostream low-temperature device operating at 193 K. Data was measured using ω scans of 0.3° per frame; each frame was exposed to X-rays for 30 seconds. A total of 1271 frames, covering a hemisphere, were collected with a maximum resolution of 0.76 Å. The first 50 frames were recollected at the end of data collection to monitor for decay. Cell

parameters were retrieved using SMART software and refined using the program SAINT on all observed reflections. Data reduction was performed using the program SAINT and absorption corrections were applied using the SADABS multiscan technique. The structures were solved by the direct methods and refined by the least squares methods on F^2 using the program SHELXL-97 incorporated in SHELXTL-PC (version 6.10). Figure 15 shows the overall packing structure of the 25AMP/3-Cl-BA cocrystal.

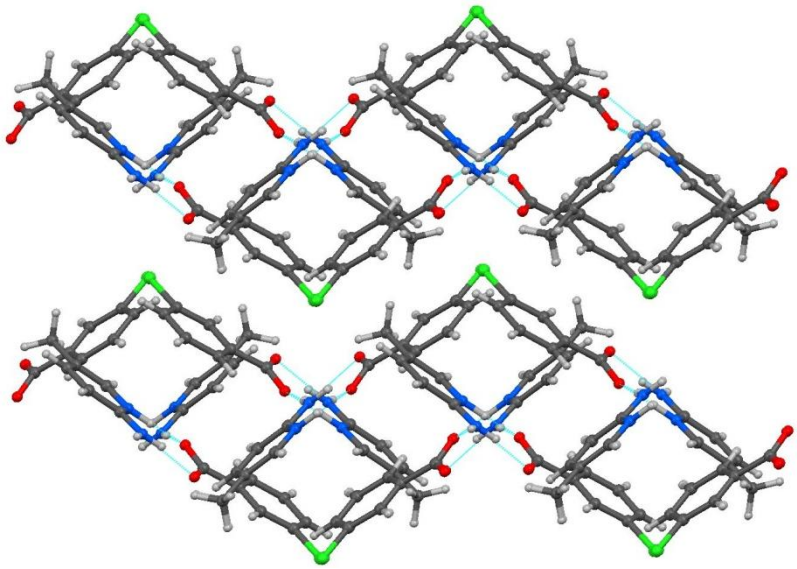

Figure 15. Crystal structure of the AMP/3-Cl-BA cocrystal. Note the hydrogen bonds between the acid and aminopyridine moieties.

This specific packing motif seen in 25AMP/3-Cl-BA cocrystal is much more general. In fact, SXRD data for all eight cocrystal studies returned the same packing orientation. This is independent of both the position of substitution on the benzoic acid moieties as well as the functional group present.

To understand how specific crystal structures attain an overall packing the interactions between moieties must be understood. Figure 16 shows the supermolecule utilizing our selected synthon, as found within in the crystal.

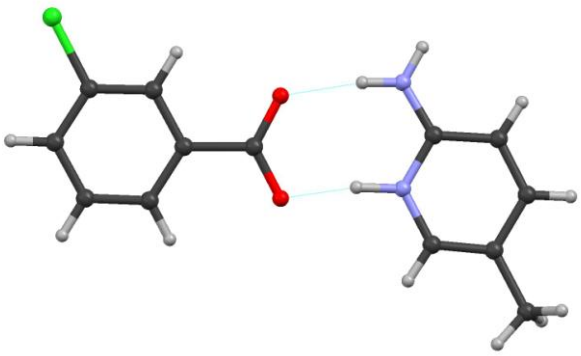

Figure 16. Aminopyridinium-carboxylate dimer. The hydrogen from the benzoic acid has transferred to the pyridine creating this charge-assisted supramolecular synthon.

This charge assisted supramolecular synthon and data supporting its existence in our experiments will be covered more extensively in discussion of specific experimental results.

The acid-aminopyridine dimer repeats in chains, alternating their orientation at nearly perpendicular angles to one another. These dimer pairs are connected by another hydrogen bond between a carboxylate oxygen atom (also associated with the pyridine nitrogen) and the second amine proton not involved in the two-point synthon. These dimer chains can be seen in Figure 17.

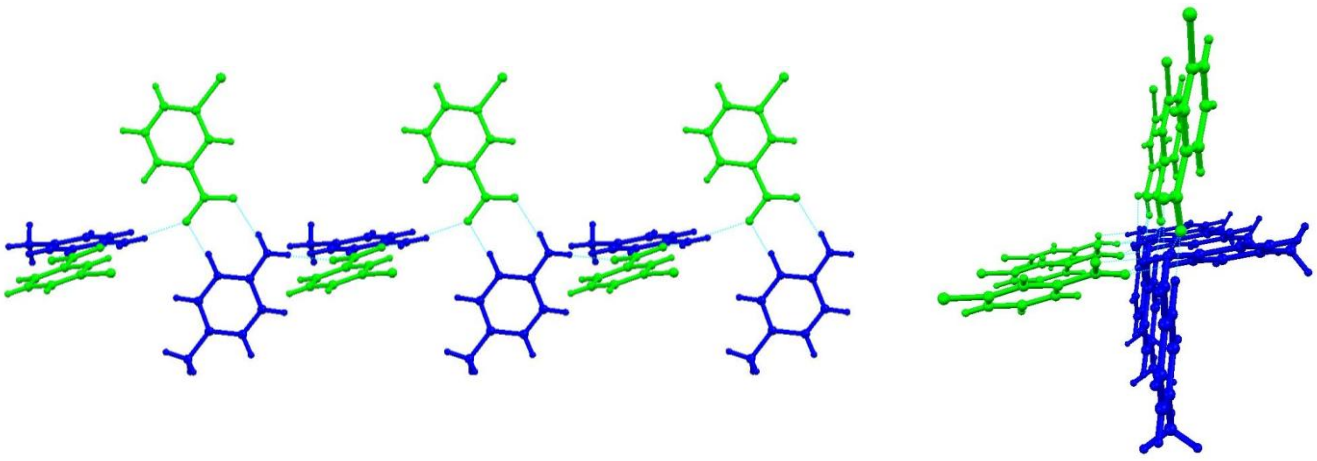

Figure 17. Dimer chains at a glance. Left: Supermolecules consisting of 3-chlorobenzoic acid (green) and 2-amino-5-methylpyridine (blue) align along a common axis, alternating in a nearly perpendicular fashion. Right: The dimer chain shown down the *c*-axis of the unit cell.

Along with the hydrogen bonds, dimer chains associate with one another through other interactions to minimize lattice energy and empty space. Two dimer chains are shown in Figure 18. Specific observations and measurements from SXRD data will be discussed within the experimental data section for each cocrystal. Using the background from this 25AMP:3-Cl-BA cocrystal we can fully explore the structural and other characteristics of the multicomponent solids prepared in this work.

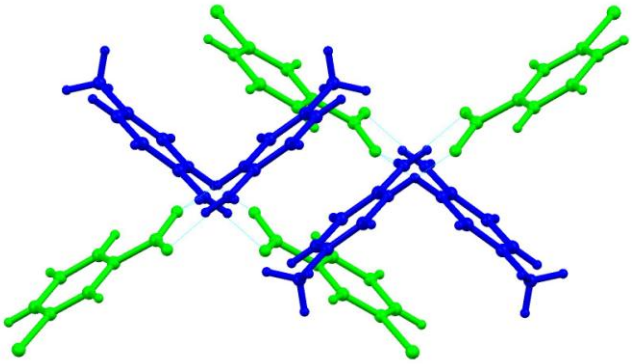

Figure 18. Two chains intertwine to minimize lattice energy and empty space. Benzoic Acids are shown in green, pyridines in blue.

Now that the methods of characterization have been explained it is now possible to present our findings. Unit cell data for all of the cocrystal structures is given in Table 7.

Table 7. Unit cell data for cocrystals of 25AMP with 3-X-and 4-X- benzoic acids.

Compound	Space group	a [Å]	b [Å]	c [Å]	α [°]	β [°]	γ [°]	Volume [Å^3]
25AMP / 3-Cl-BA	$P2_1/c$	9.1357	11.609	12.128	90	101.522	90	1260.33
25AMP / 3-CH_3-BA	$P2_1/c$	10.2358	11.0111	12.0603	90	113.881	90	1242.91
25AMP / 3-Br-BA	$P2_1/c$	9.2746	11.696	12.134	90	100.999	90	1292.07
25AMP / 3-I-BA	$P2_1/c$	9.55	11.85	12.17	90	100.72	90	1353.21
25AMP / 4-Cl-BA	$P2_1/c$	9.68	10.7758	12.1614	90	102.523	90	1238.37
25AMP / 4-CH_3-BA	$P2_1/c$	9.7375	10.8644	12.1685	90	104.024	90	1248.96
25AMP / 4-Br-BA	$P2_1/c$	9.7634	10.8605	12.2162	90	101.227	90	1270.56
25AMP / 4-I-BA	$P2_1/c$	9.9498	10.9834	12.3259	90	99.877	90	1327.04

3.5. Binary Cocrystals

3.5.1. 25AMP:3-Cl-BA (1:1)

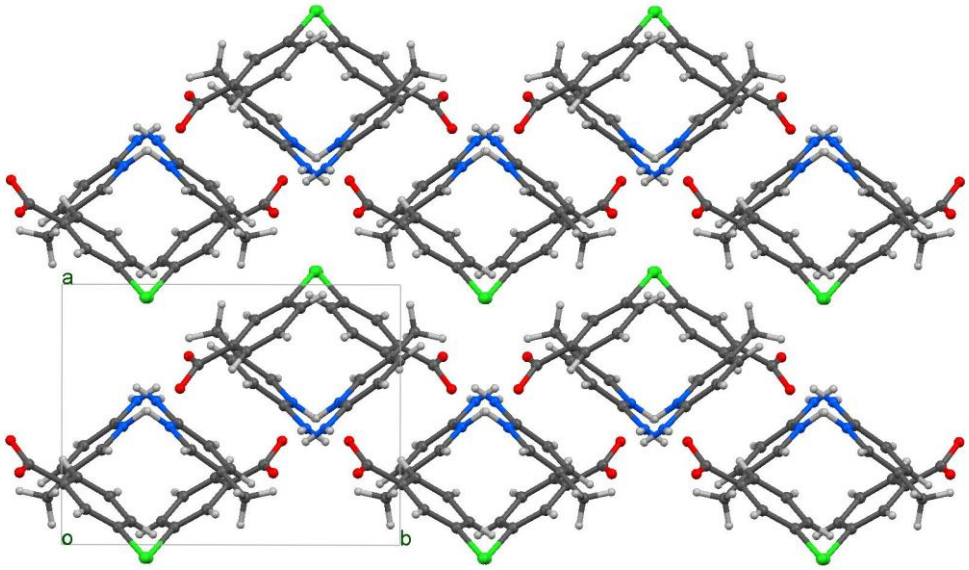

Figure 19. Crystal structure of 25AMP:3-Cl-BA (1:1).

SXRD data collected on the 25AMP/3-Cl-BA 1:1 cocrystal confirmed the existence of both components in one crystal. The two components are assembled through hydrogen bonding between the carboxylic acid and aminopyridine groups. The bond lengths and angles about the supramolecular synthon imply a proton transfer from the carboxylic acid group to the pyridine. An increase in the C-N-C bond angle within the pyridine ring gives the first indication that the benzoic acid hydrogen has migrated to the base.[18, 28, 29] The endocyclic C-N-C bond angle for neutral 25AMP is 117.50°.[30] SXRD data reveals a value of 122.04° for the 1:1 cocrystal 25AMP/3-Cl-BA. This is consistent with the C-N-C bond angle found in the 2-amino-pyridinium chloride salt which measures at 123.59°.[31]

The carbon-oxygen bond lengths of the carboxylic acid group are another indication that the cocrystallization involves a proton transfer. Literature values for neutral C-O and C=O bonds for carboxylic acids attached to a phenyl ring are listed at 1.305 Å and 1.226 Å, respectively, while the C-O bond lengths for deprotonated

carboxylate groups are nearly symmetrical at 1.255 Å.[29] The 25AMP:3-Cl-BA 1:1 cocrystal shows bond lengths of 1.245 Å and 1.266 Å, again in agreement with the presence of a deprotonated carboxylate moiety.

Previously, we discussed the intricate associations between chains of dimers oriented along the *c*-axis of the unit cell. Two chains intertwine to reduce the overall volume while utilizing π–π stacking interactions help stabilize the crystal structure. Two distinct π-π interactions are observed between these dimer chains. The pyridine moieties stack with acids from adjacent chains at a distance of 3.997 Å while pyridines from separate chains stack at 3.510 Å.

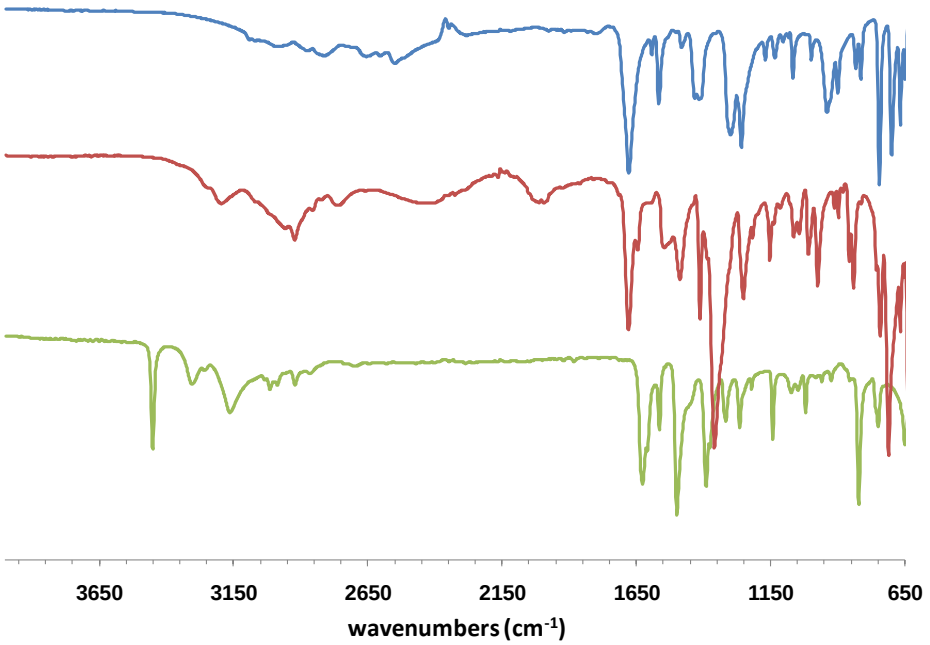

Figure 20. Stacked FTIR spectra of 25AMP, 3-Cl-BA, and the respective cocrystal. 25AMP (green), 3-Cl-BA (blue), cocrystal (red).

FTIR spectra for the 1:1 25AMP/3-Cl-BA cocrystal, 25AMP, and 3-Cl-BA are unique. The 25AMP spectrum include as peak at 1627 cm^{-1} consistent with conjugated C-C/C-N stretching within the pyridine ring while 3-Cl-BA peak situated at 1687 cm^{-1}, characteristic of carbonyl C=O stretching when the functional group is conjugated with an aromatic ring. The FTIR spectrum for our cocrystal includes peaks at 1679 cm^{-1} and

1359 cm^{-1}, the former consistent with asymmetrical stretching of the carboxylate moiety as well as the continued presence of conjugated C-C and C-N stretching, while the latter is consistent with symmetrical carboxylate stretching. All of these observations are consistent with SXRD data depicting a charge assisted supramolecular synthon via proton transfer.

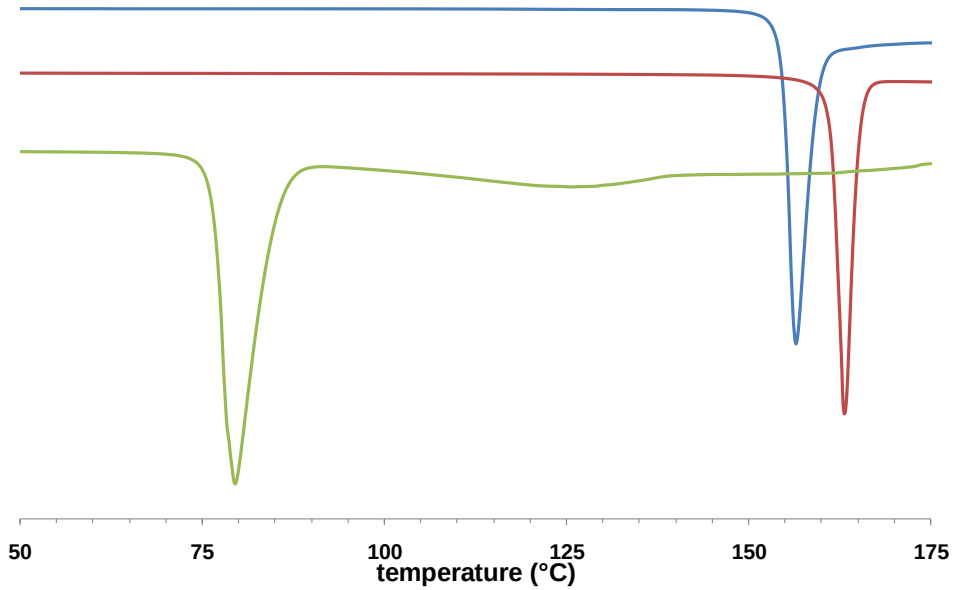

Figure 21. Stacked DSC endotherms of 25AMP, 3-Cl-BA, and the respective cocrystal. 25AMP (green), 3-Cl-BA (blue), cocrystal (red).

Thermal analysis of the 25AMP/3-Cl-BA 1:1 cocrystal and its respective substituents concur with previous data depicting the presence a unique crystalline product. 25AMP, 3-Cl-BA, and the 1:1 cocrystal exhibit melting points 79.4 °C, 156.4 °C, and 163.1 °C, respectively.

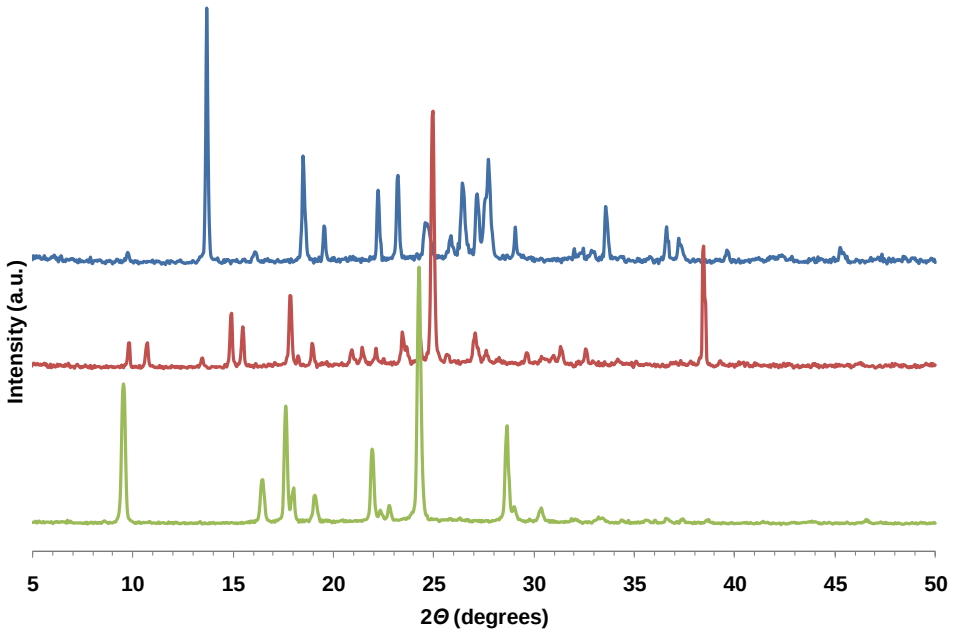

Figure 22. Stacked PXRD data for 25AMP, 3-Cl-BA, and the respective cocrystal. 25AMP (green), 3-Cl-Ba (blue), cocrystal (red).

Figure 22 shows the PXRD patterns of the 25AMP:3-Cl-BA cocrystal with the two individual components. As a finger-print match, we can se the cocrystal give a diffraction pattern that is distinct from the components. This derivation suggests that the crystals we obtained are not a physical mixture of the components. On the other hand the pattern matches very well with the pattern calculated from single-crystal X-ray data (not shown). This matching indicates the bulk sample has the same solid state structure as the crystal selected for single-crystal X-ray studies.

3.5.2. 25AMP:3-CH_3-BA (1:1)

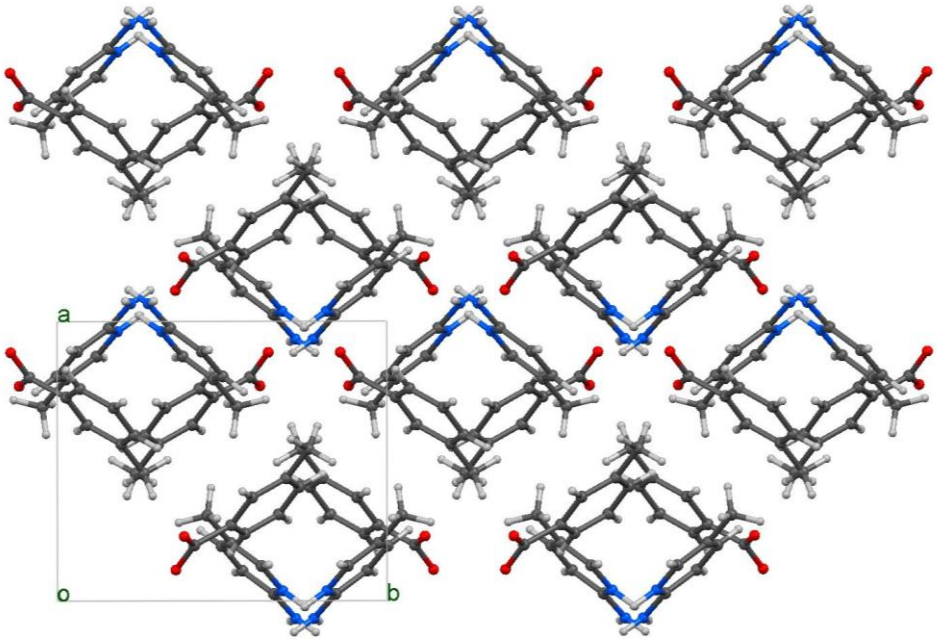

Figure 23. Crystal structure of 1:1 25AMP/3-CH_3-BA. Notice the gross structural similarity between this cocrystal and the 25AMP:3-Cl-BA crystal shown in Figure 19.

Single crystal X-ray diffraction data of 1:1 25AMP/3-CH_3-BA is also consistent with a charge assisted binary cocrystal. The endocyclic C-N-C bond angle of the aminopyridine moiety measures 121.81° and the carboxylate C-O bond lengths are 1.247 Å and 1.268 Å. π-π stacking distances between aminopyridine rings of 3.347 Å and 3.718 Å between aminopyridine and acid moieties are also analogous to the crystal structure of the 1:1 25AMP/3-Cl-BA cocrystal.

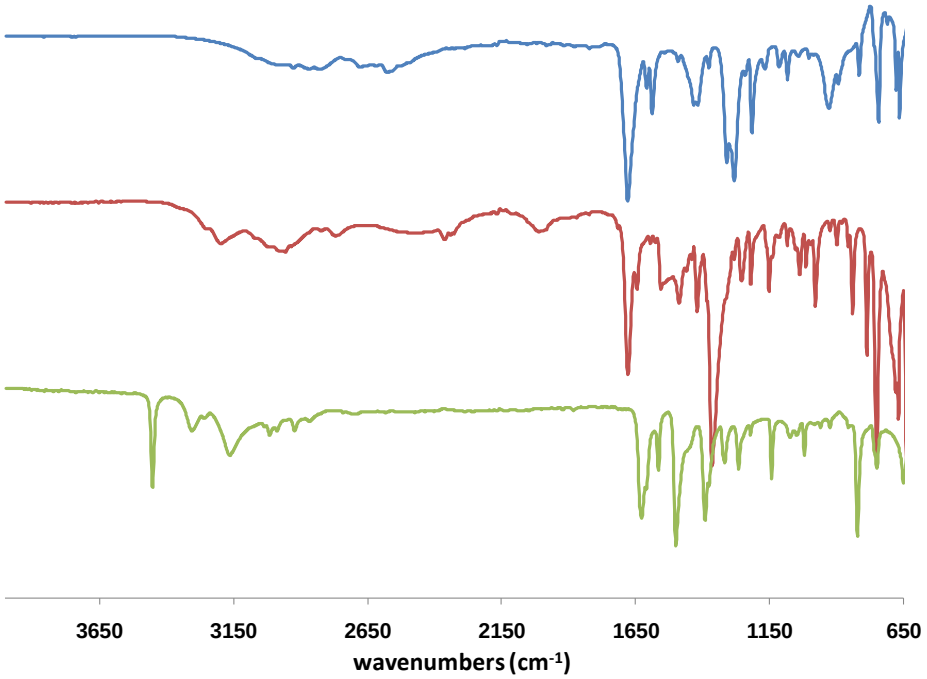

Figure 24. Stacked FTIR spectra of 25AMP, 3-CH3-BA, and the respective cocrystal. 25AMP (green), 3-CH3-BA (blue), cocrystal (red).

FTIR spectra for 25AMP, 3-CH3-BA, and the 1:1 cocrystal preserve the presence of three different materials. This cocrystal FTIR spectrum also exhibits the strong carboxylate asymmetrical stretching/conjugated C-C and C-N stretching peak at 1679 cm^{-1} and a peak at 1365 cm^{-1} consistent with carboxylate symmetric stretching.

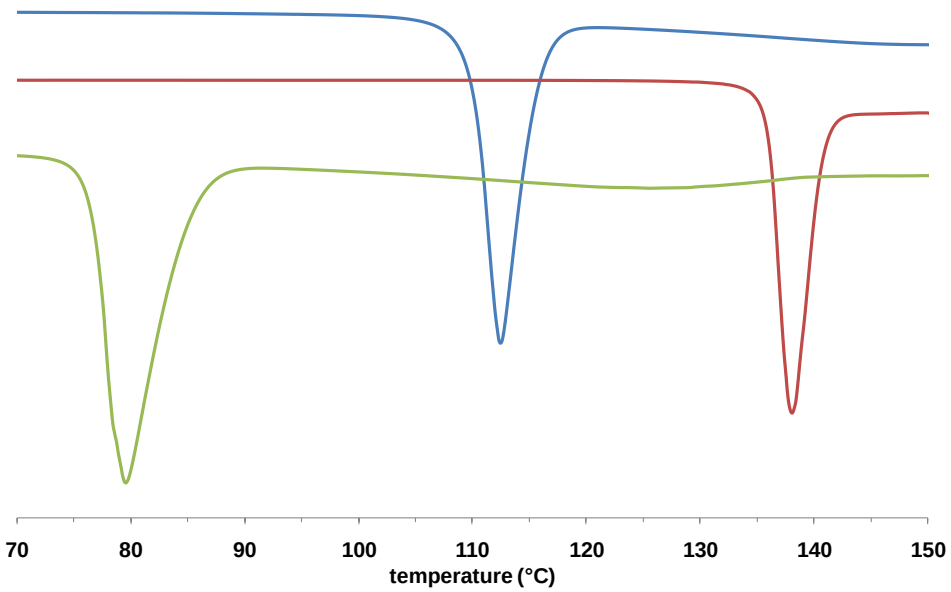

Figure 25. Stacked DSC thermograms of 25AMP, 3-CH_3-BA, and the respective cocrystal. 25AMP (green), 3-CH_3-BA (blue), cocrystal (red).

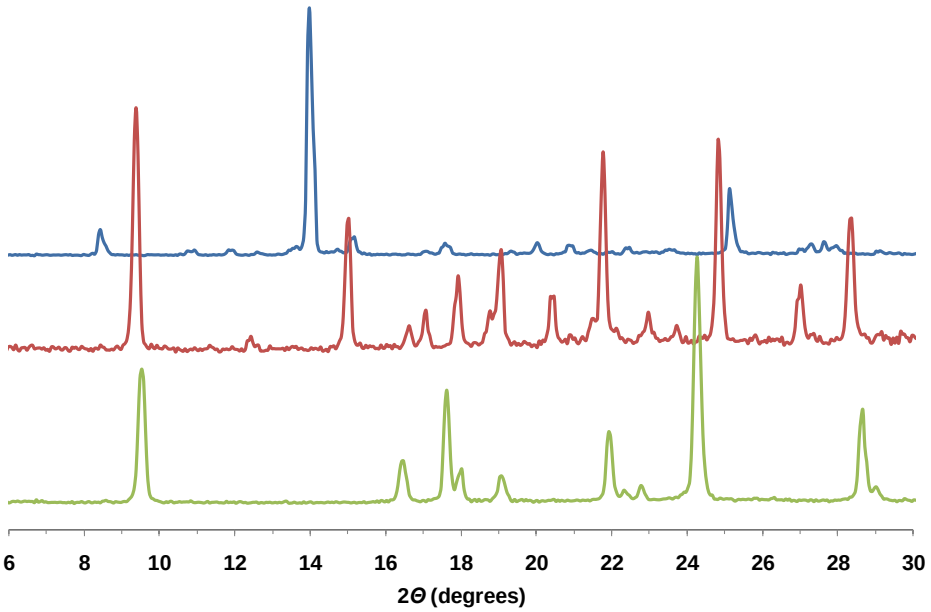

Figure 26. Stacked PXRD data for 25AMP, 3-CH_3-BA, and the respective 1:1 cocrystal. 25AMP (green), 3-CH_3-BA (blue), cocrystal (red).

DSC analysis depicts melting points for 25AMP, 3-CH_3-BA, and the 1:1 25AMP/3-CH_3-BA cocrystal at 79.4°C, 112.4°C, and 138.0 °C, respectively. Note that in

this case the cocrystal has a melting point nearly 26 °C higher than that of its most thermally stable substituent 3-CH_3-BA.

Figure 26 shows the PXRD patterns of 25AMP, 3-CH3-BA, and the 1:1 25AMP:3-CH_3-BA cocrystal. The diffraction pattern collected from the cocrystal confirms the sample is neither individual components nor a physical mixture. However, the PXRD data is consistent with the diffraction pattern generated by single-crystal X-ray diffraction data, confirming the bulk PXRD sample has the same crystal structure as the crystal selected for SXRD

3.5.3. 25AMP:3-Br-BA (1:1)

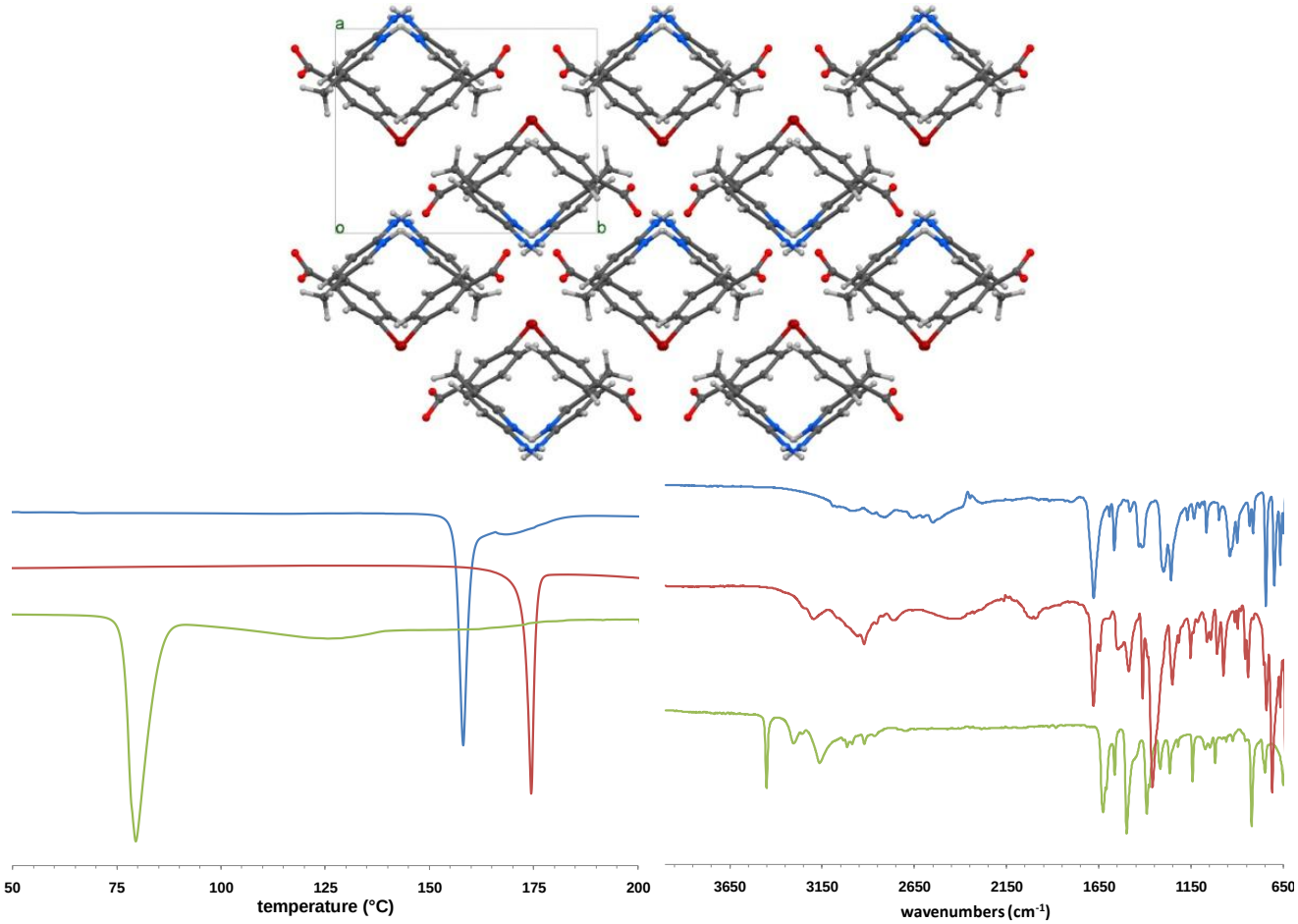

Figure 27. SXRD, DSC, and FTIR data for 1:1 25AMP/3-Br-BA. Graphed data has been color coded: 25AMP (green), 3-Br-BA (blue), cocrystal (red).

The crystal structure of the 1:1 25AMP/3-Br-BA cocrystal depicts another charge assisted supramolecular synthon. Aminopyridine C-N-C bond angle measures 122.2°, carboxylate C-O bonds measure 1.243 Å and 1.265 Å, and π-π stacking interactions measure 3.549 Å and 4.064 Å for pyridine-pyridine and pyridine-acid rings, respectively. Thermal analysis by DSC returned melting points of 79.4°C for 25AMP, 158.0°C for 3-Br-BA, and 174.4°C for the 1:1 cocrystal.

FTIR data collected for 1:1 25AMP/3-Br-BA shows evidence of symmetric carboxylate stretching at 1359 cm^{-1} and asymmetrical carboxylate stretching at 1681 cm^{-1}. These values continue to be analogous with previously observed cocrystals utilizing a charge assisted supramolecular synthon.

3.5.4. 25AMP:3-I-BA (1:1)

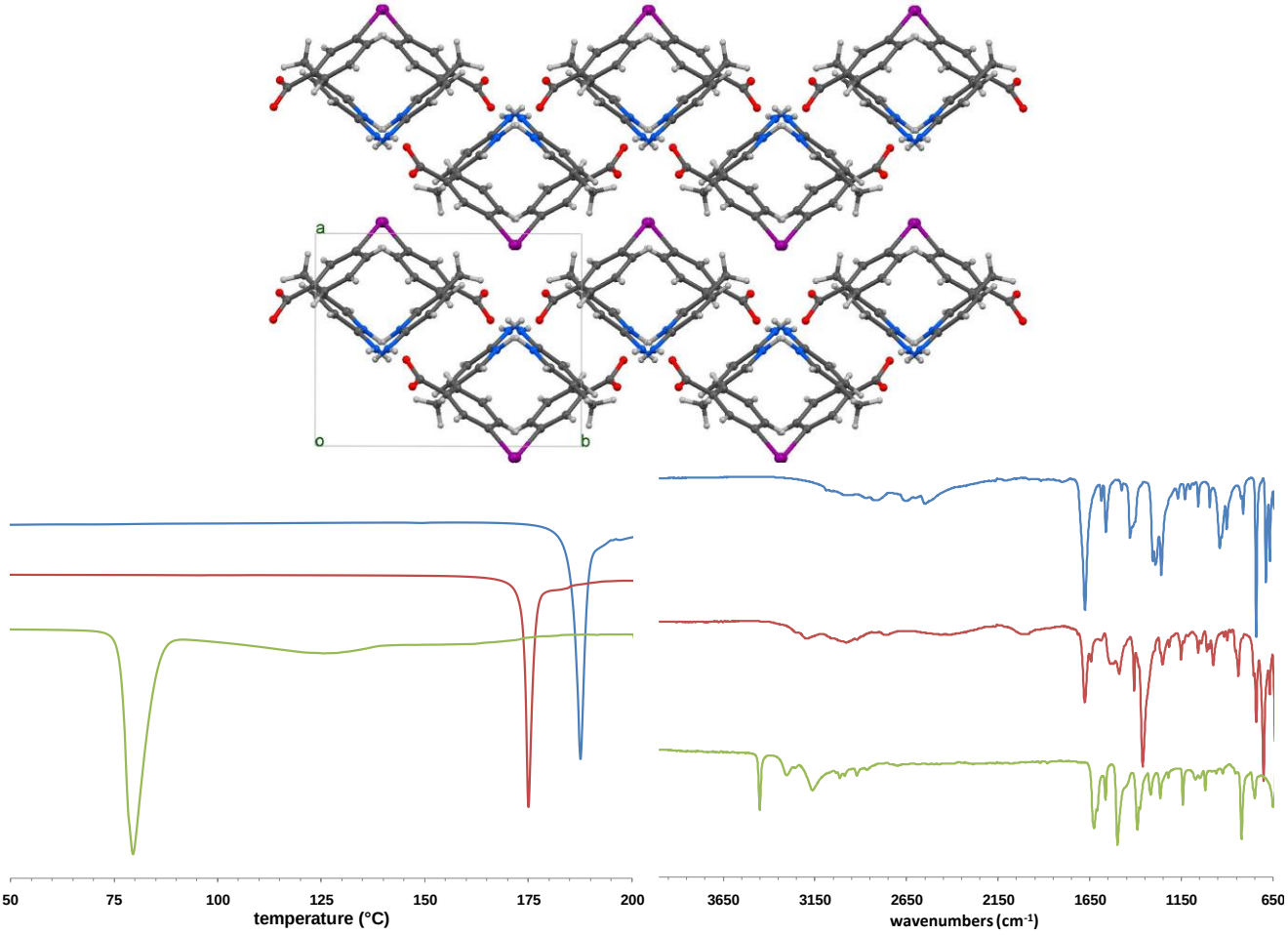

Figure 28. SXRD, DSC, and FTIR data for 1:1 25AMP/3-I-BA. Graphed data has been color coded: 25AMP (green), 3-I-BA (blue), cocrystal (red).

Data collected from the 1:1 25AMP/3-I-BA cocrystal are analogous to previous experiments. SXRD and FTIR analysis gives values consistent with charge assisted cocrystallization: endocyclic C-N-C bond angle is 121.68°, carboxylate C-O bond lengths measure 2.779 Å and 2.671 Å, and pyridine-pyridine and pyridine-acid π-π stacking distances are 3.743 Å and 4.162 Å, respectively, while symmetric carboxylate stretching and asymmetric carboxylate stretching peaks are observed at 1361 cm^{-1} and 1679 cm^{-1}. Thermal analysis with DSC gave melting points of 79.4°C for 25AMP, 174.9°C for the cocrystal, and 187.4°C for 3-I-BA.

3.5.5. 25AMP:4-Cl-BA (1:1)

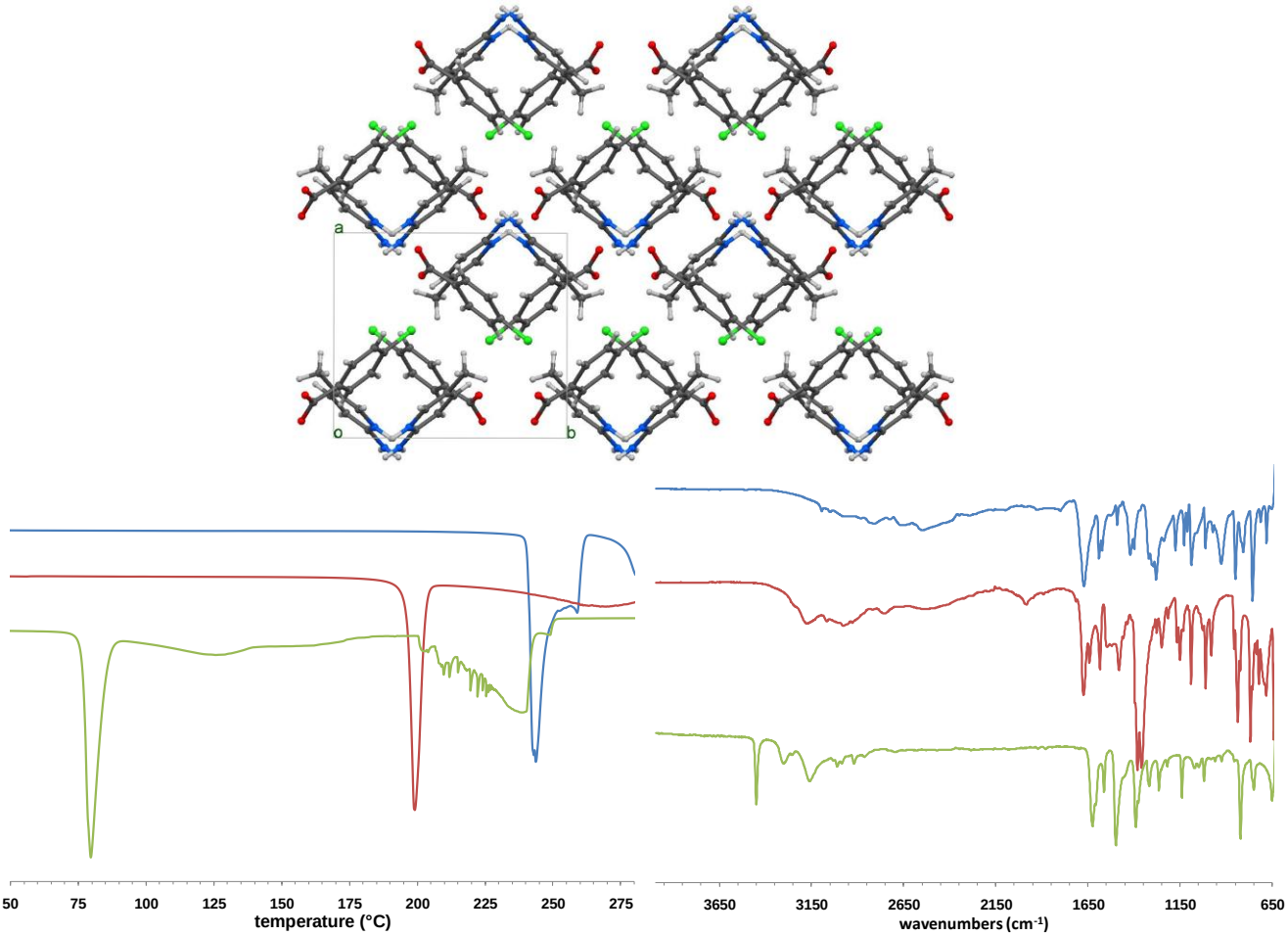

Figure 29. SXRD, DSC, and FTIR data for 1:1 25AMP/4-Cl-BA. Graphed data has been color coded: 25AMP (green), 4-Cl-BA (blue), cocrystal (red). Characterization data is given in Table 8.

Table 8. Characterization data for 1:1 25AMP/4-Cl-BA.

	SXRD				FTIR		DSC
	C-N-C Bond Angle (deg)	C-O Bond Lengths (angstroms)	Pyr-Pyr Stack Dist. (angstroms)	Pyr-Acid Stack Dist. (angstroms)	Carboxylate Sym. Stretch (cm^{-1})	Carboxylate Asym. Stretch (cm^{-1})	m.p. (C)
25AMP	-	-	-	-	-	-	79.4
cocrystal	121.99	2.742, 2.722	3.408	3.804	1359	1678	199
4-Cl-BA	-	-	-	-	-	-	243.6

3.5.6. 25AMP:4-CH_3-BA (1:1)

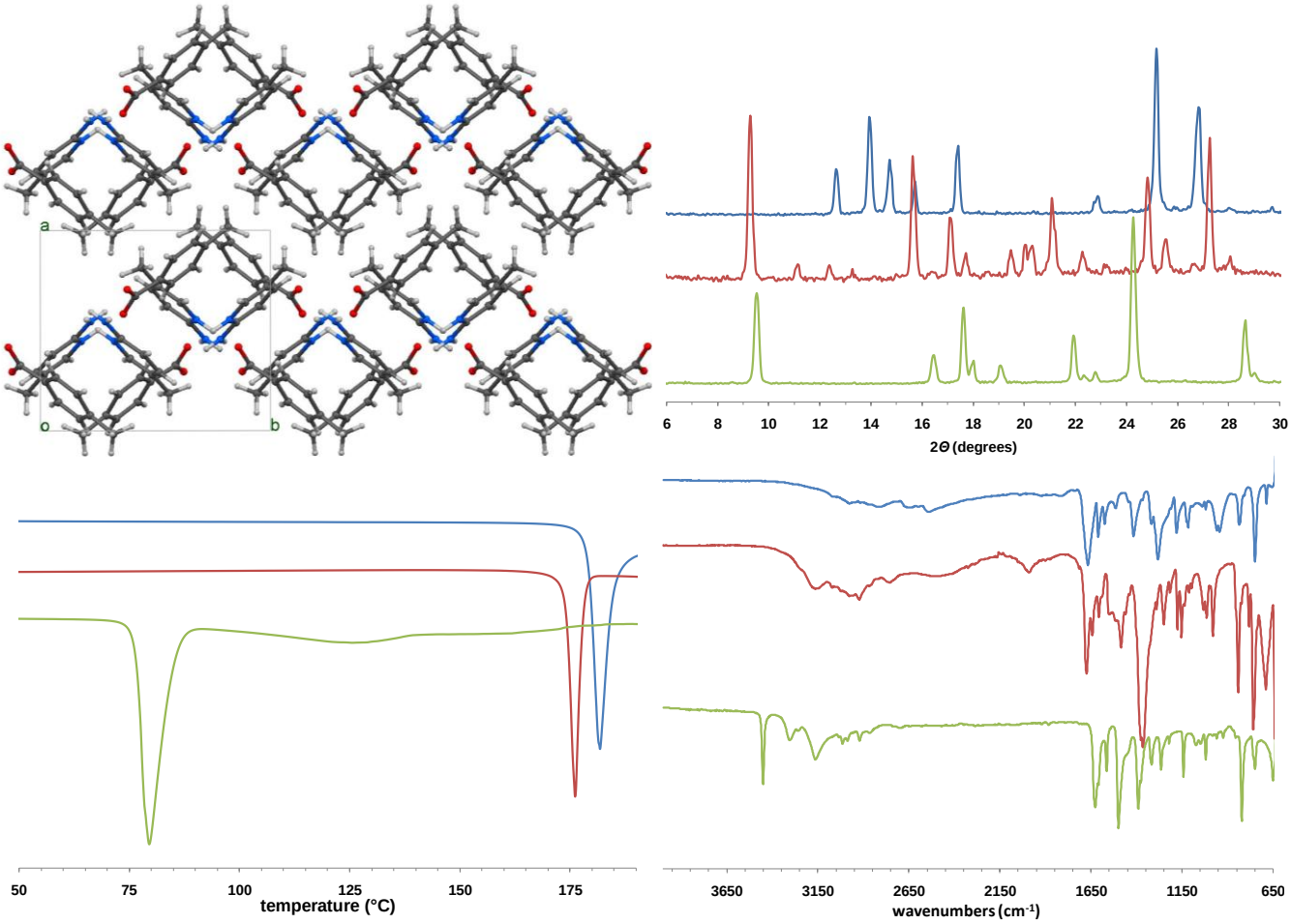

Figure 30. SXRD, PXRD, DSC, and FTIR data for 1:1 25AMP/4-CH_3-BA. Graphed data has been color coded: 25AMP (green), 4-CH_3-BA (blue), cocrystal (red).

PXRD data for 25AMP:4-CH_3-BA continues to depict a crystalline product unique from individual components and consistent with SXRD studies. Table 9 contains pertinent data from SXRD, FTIR, and DSC characterization.

Table 9. SXRD, FTIR, and DSC data for 1:1 25AMP/4-CH_3-BA.

	SXRD				FTIR		DSC
	C-N-C Bond Angle (deg)	C-O Bond Lengths (angstroms)	Pyr-Pyr Stack Dist. (angstroms)	Pyr-Acid Stack Dist. (angstroms)	Carboxylate Sym. Stretch (cm^{-1})	Carboxylate Asym. Stretch (cm^{-1})	m.p. (C)
25AMP	-	-	-	-	-	-	79.4
cocrystal	121.96	2.744, 2.720	3.430	3.804	1367	1676	176
4-CH3-BA	-	-	-	-	-	-	181.7

3.5.7. 25AMP:4-Br-BA (1:1)

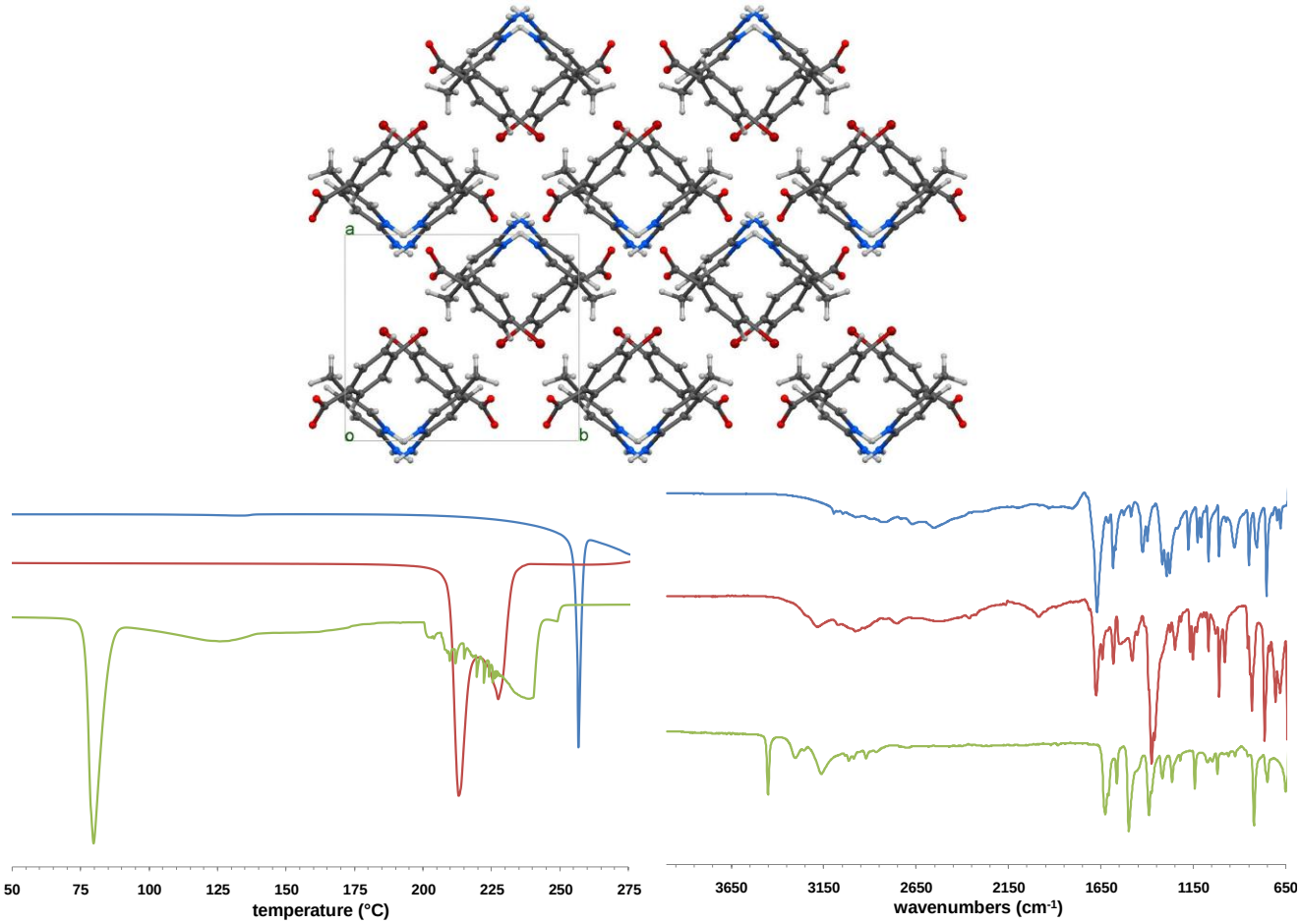

Figure 31. SXRD, PXRD, DSC, and FTIR data for 1:1 25AMP/4-Br-BA. Graphed data has been color coded: 25AMP (green), 4-Br-BA (blue), cocrystal (red).

Note the dual endotherms present in the cocrystal DSC data. The first endotherm represents the cocrystal melting. The second endotherm is most likely associated with the melting of 4-Br-BA which is precipitating to a solid as the cocrystal melts.

Table 10. Characterization data for 1:1 25AMP/4-Br-BA.

	SXRD				FTIR		DSC
	C-N-C Bond Angle (deg)	C-O Bond Lengths (angstroms)	Pyr-Pyr Stack Dist. (angstroms)	Pyr-Acid Stack Dist. (angstroms)	Carboxylate Sym. Stretch (wavenumbers)	Carboxylate Asym. C-C/C-N Stretch (wavenumbers)	m.p. (C)
25AMP	-	-	-	-	-	-	79.4
cocrystal	122.46	2.755, 2.727	3.440	3.808	1361	1678	212.9
4-Br-BA	-	-	-	-	-	-	256.6

3.5.8. 25AMP:4-I-BA (1:1)

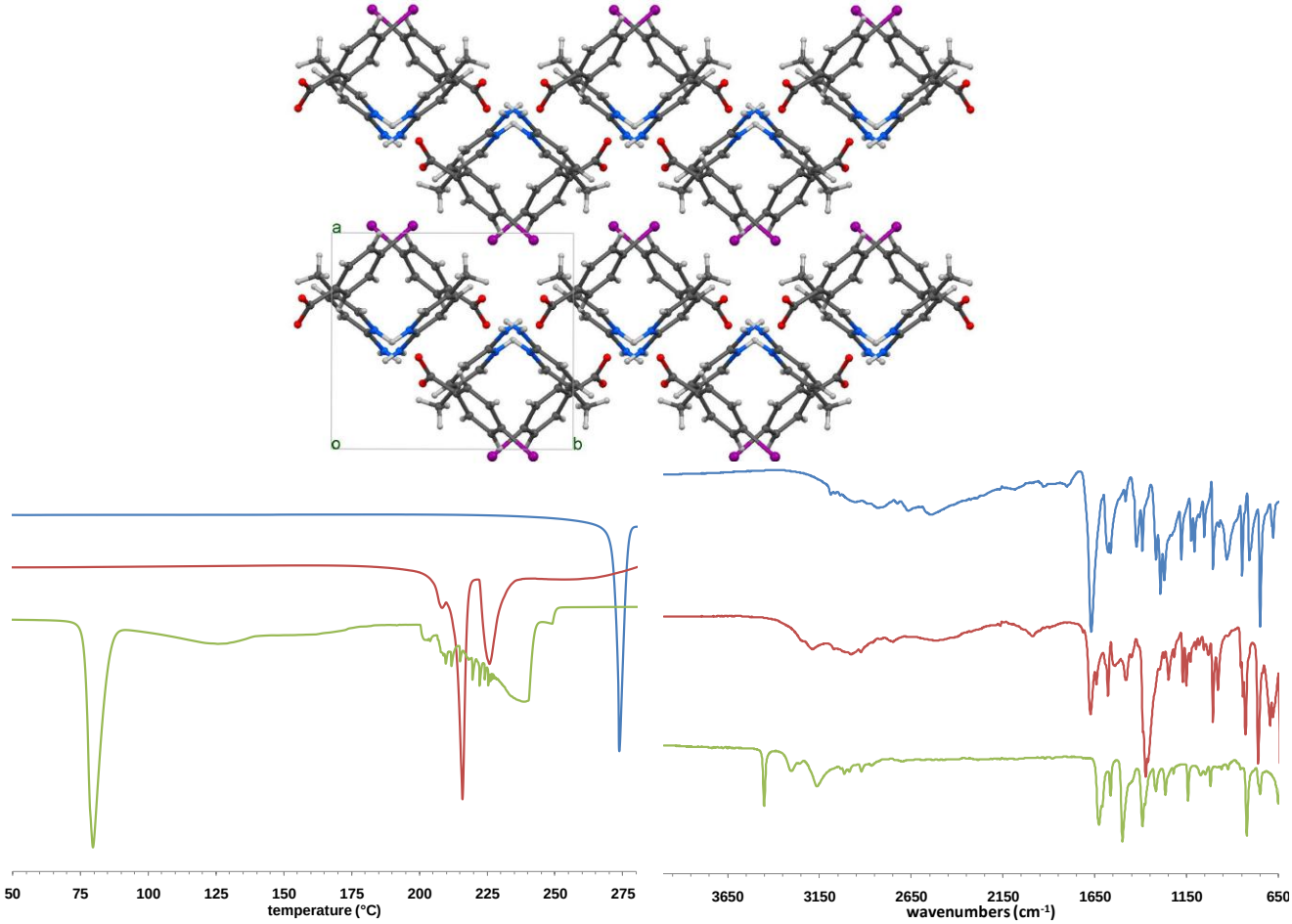

Figure 32. SXRD, PXRD, DSC, and FTIR data for 1:1 25AMP/4-I-BA. Graphed data has been color coded: 25AMP (green), 4-I-BA (blue), cocrystal (red).

Table 11. Characterization data for 1:1 25AMP/4-I-BA.

	SXRD				FTIR		DSC
	C-N-C Bond Angle (deg)	C-O Bond Lengths (angstroms)	Pyr-Pyr Stack Dist. (angstroms)	Pyr-Acid Stack Dist. (angstroms)	Carboxylate Sym. Stretch (cm^{-1})	Carboxylate Asym Stretch (cm^{-1})	m.p. (C)
25AMP	-	-	-	-	-	-	79.4
cocrystal	121.66	2.759, 2.718	3.571	3.871	1373	1676	215.9
4-I-BA	-	-	-	-	-	-	273.6

3.6. Ternary Solid Solutions

3.6.1. Equimolar Acid Studies

Unit cell data collected for equimolar ternary solid solution experiments show our aminopyridine-benzoic acid systems continue to exhibit the $P2_1/c$ space group with increasing number of benzoic acid components. Unit cell volumes for the experiments are comparable to those of cocrystals of 25AMP with the individual benzoic acids present (i.e. – the 25AMP/3-Cl-BA/3-I-BA ternary product (1314 $Å^3$) is close to the average volumes of the 25AMP/3-Cl-BA and 25AMP/3-I-BA cocrystals (1260.33 $Å^3$ + 1353.21 $Å^3/2$ = 1306.77 $Å^3$) Table 12 contains the unit cell data for the equimolar ternary solid solution experiments.

Table 12. Structural data for ternary solid solutions with equimolar acid ratios.

Compound	Space group	a [Å]	b [Å]	c [Å]	α [°]	β [°]	γ [°]	Volume [$Å^3$]
25AMP / 3-Cl-BA / 3-CH_3-BA	-	-	-	-	-	-	-	-
25AMP / 3-Cl-BA / 3-Br-BA	$P2_1/c$	9.136	11.552	12.044	90	101.231	90	1246.771
25AMP / 3-Cl-BA / 3-I-BA	$P2_1/c$	9.3969	11.7093	12.1552	90.0735	100.6598	90.009	1314.368
25AMP / 3-CH_3-BA / 3-Br-BA	-	-	-	-	-	-	-	-
25AMP / 3-CH_3-BA / 3-I-BA	$P2_1/c$	10.222	10.941	12.011	90	114.012	90	1227.048
25AMP / 3-Br-BA / 3-I-BA	$P2_1/c$	9.4046	11.7808	12.1419	90	100.8151	90	1321.347
25AMP / 4-Cl-BA / 4-CH_3-BA	$P2_1/c$	9.67	10.769	12.13	90	103.03	90	1230.648
25AMP / 4-Cl-BA / 4-Br-BA	$P2_1/c$	9.7239	10.8234	12.192	90	101.6904	90	1256.543
25AMP / 4-Cl-BA / 4-I-BA	$P2_1/c$	9.763	10.799	12.158	90	101.139	90	1257.678
25AMP / 4-CH_3-BA / 4-Br-BA	$P2_1/c$	9.639	10.744	12.063	90	103.86	90	1212.888
25AMP / 4-CH_3-BA / 4-I-BA	$P2_1/c$	9.869	11.0768	12.1264	90	102.7675	90	1292.839
25AMP / 4-Br-BA / 4-I-BA	$P2_1/c$	9.76	10.798	12.128	90	100.427	90	1257.044

Note: Unit cell data was not collected for the 25AMP/3-Cl-BA/3-CH3-BA and 25AMP/3-CH3-BA/3-Br-BA solid solutions.

While thermal analysis of the twelve ternary solid solution products does not confirm the relative ratios of the benzoic acid components crystallized in each system, it is an efficient way of proving that each crystal is different. DSC data for all ternary crystallization products showed twelve distinct melting points that did not match melting points of products showed twelve that did not match melting points of 25AMP or corresponding benzoic acids. These 12 products also have unique melting points when compared to all of the previously reported DSC data in this paper. This means that none of these twelve products is a recrystallized raw material or a cocrystal.

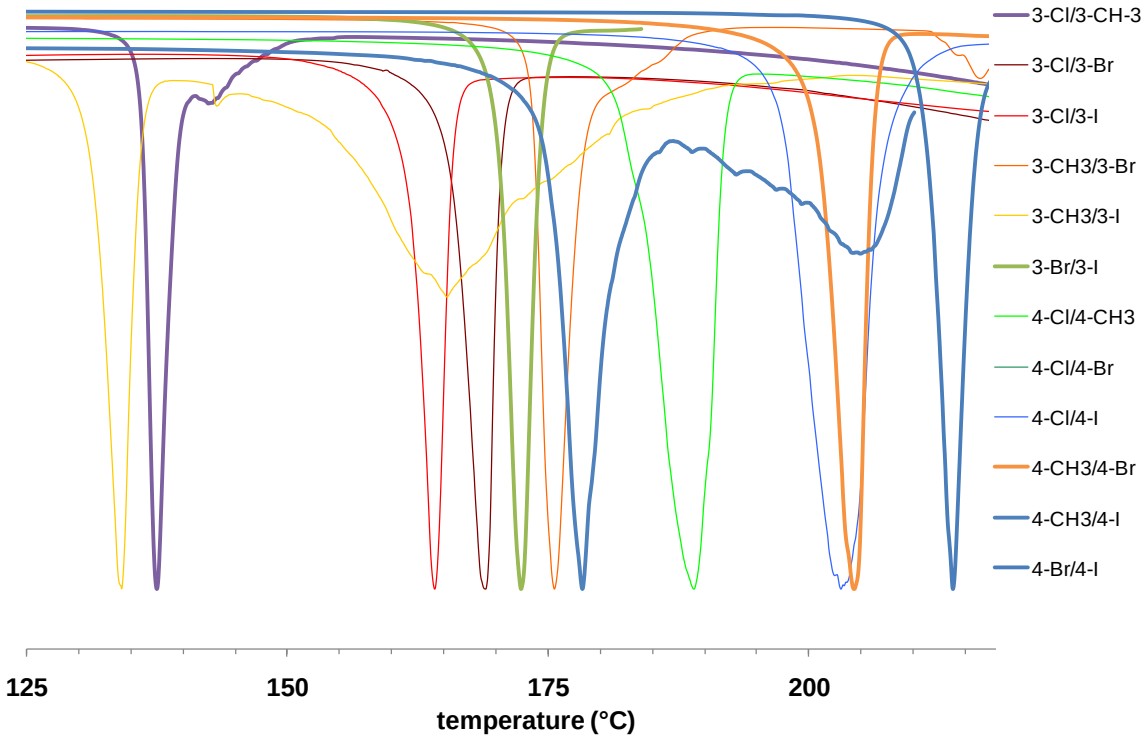

Figure 33. DSC thermograms of the ternary solid solution products with equimolar acid ratios.

3.6.2. Variable Acid Ratio Experiments

Characterization of the large scale crystallization studies depends less upon direct comparison of raw materials to crystalline products as comparing samples to samples. Data sets were collected and stacked in order to best show subtle differences in spectra and diffraction patterns giving way to visible trends.

3.6.2.1. 25AMP:3-Cl-BA:3-CH3-BA

FTIR spectra for the first large scale series depicted obvious trends in peak intensities. Some changes were subtle, with only a small peak emerging or receding as the samples increased in relative 3-CH_3-BA concentration. Others however change drastically. Figure 33 contains the eleven stacked FTIR spectra with arrows indicating changes in peak intensity.

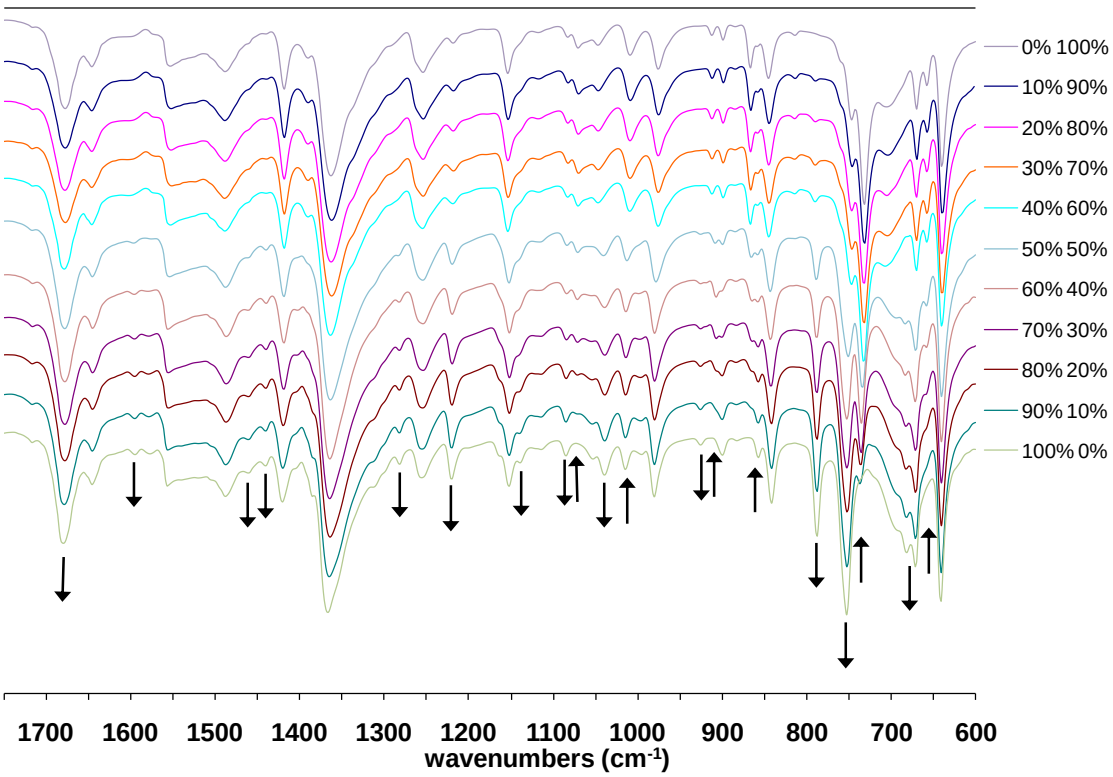

Figure 34. Stacked FTIR spectra for the 25AMP/3-CH_3-BA/3-Cl-BA series. Each solid solution is labeled in the format X% Y%: the first number indicates the percent amount of 3-CH_3-BA and the second indicates percent 3-Cl-BA. Arrows denote changes in peak intensity from top to bottom. (i.e. - down arrow marks a peak growing larger from 0% 100% to the 100% 0%)

Some of the most obvious transitions are observed when two adjacent peaks are changing simultaneously. These dual peak transitions are seen when one peak is increasing in intensity while the second is decreasing, or vice versa, making the change visually more apparent. One such trend is found at 750 cm^{-1} and 730 cm^{-1}. Only a small bump in comparison to the peak at 730 cm^{-1}, which is the largest peak found in the **0% 100%** FTIR spectrum, the 750 cm^{-1} peak increases in intensity as the ratio of 3-CH3-BA to 3-Cl-BA increases. In fact, the 750 cm^{-1} peak is the largest found in the **100% 0%** data set.

Thermal analysis of the 25AMP/3-CH_3-BA/3-Cl-BA series produced obvious trends as well (Figure 34).

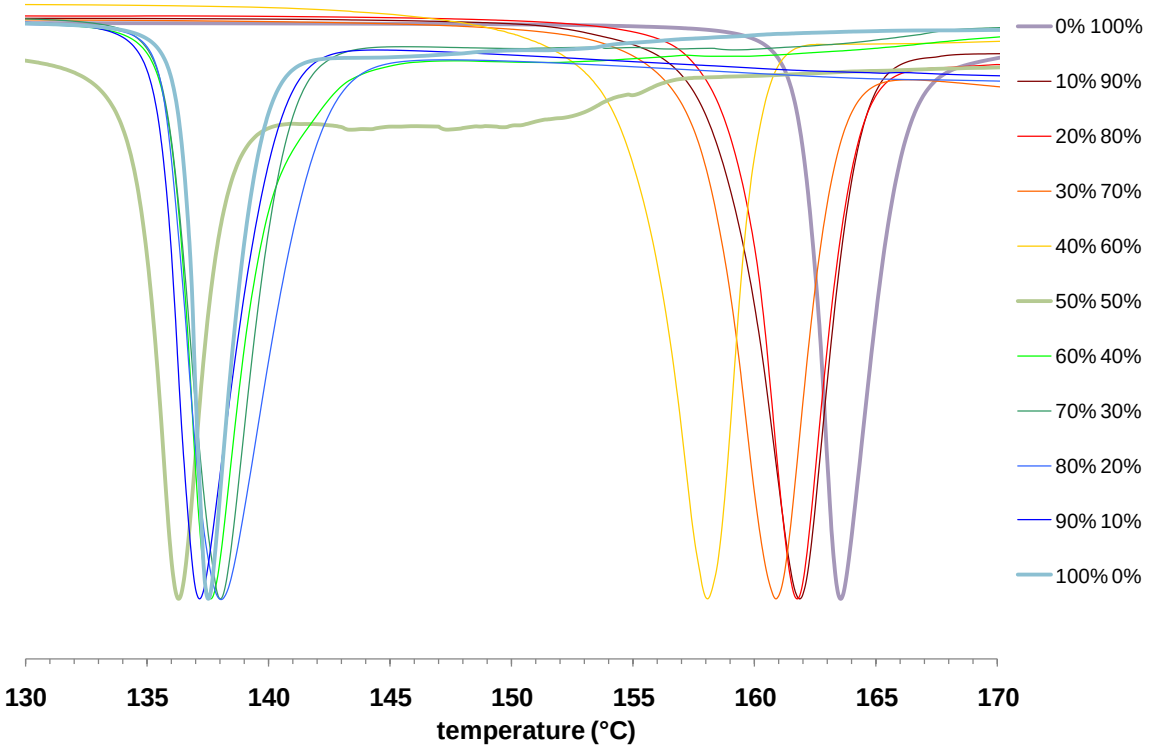

Figure 35. DSC endotherms for the 25AMP/3-CH3-BA/3-Cl-BA series. Each solid solution is labeled in the format X% Y%: the first number indicates the percent amount of 3-CH_3-BA and the second indicates percent 3-Cl-BA.

Melting points collected with DSC clustered closely to those of the cocrystals bracketing the series. In fact, **40% 60%** was the farthest melting point from either cocrystal while varying less than 6°C.

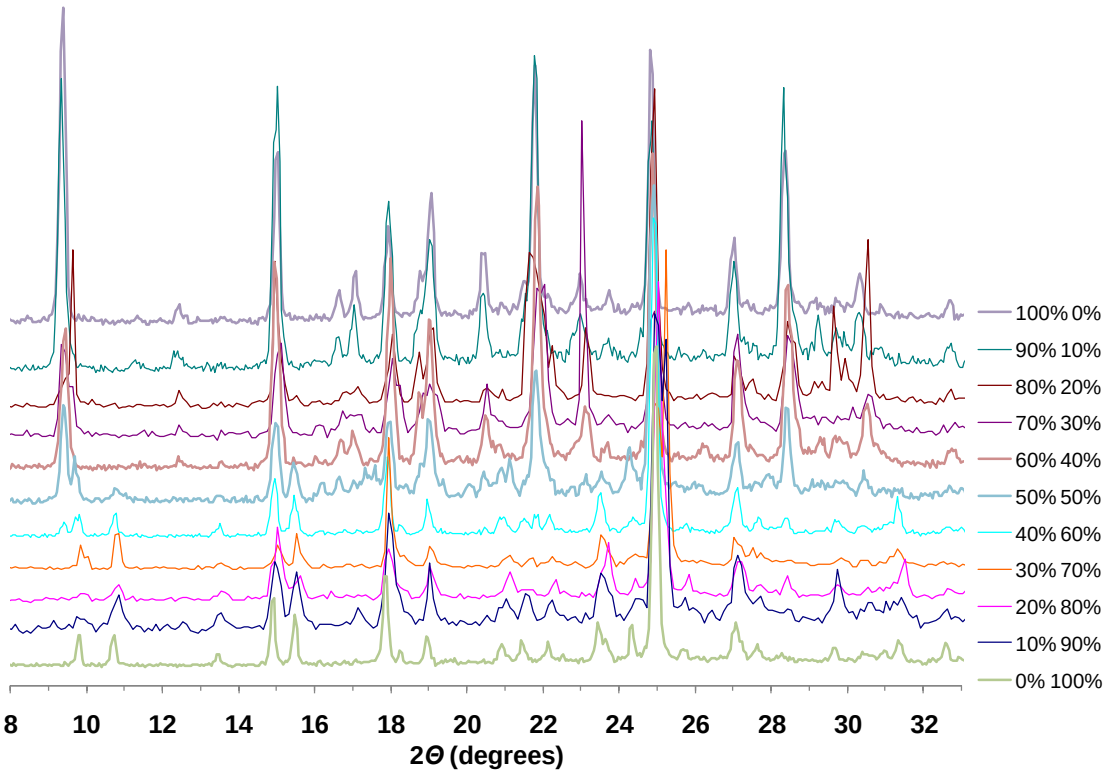

Figure 36. Stacked PXRD data for the 25AMP/3-CH3-BA/3-Cl-BA series. Each solid solution is labeled in the format X% Y%: the first number indicates the percent amount of 3-CH_3-BA and the second indicates percent 3-Cl-BA.

Gradual growth or reduction in peak intensities shown in PXRD data clearly indicates the continuous change in contents. Small shifts in peak location (i.e. change in 2Θ) indicate that the crystals are supramolecular solid solutions and not physical mixtures of two separate cocrystals.

At 9.4° a peak recedes to baseline from **100% 0%** to **0% 100%**. This peak, consistent with the (100) reflection of the 25AMP/3-CH3-BA cocrystal has no corresponding peak in the PXRD pattern for 25AMP/3-Cl-BA, thus the smooth transition to baseline as the relative ratio of 3-CH_3-BA to 3-Cl-BA decreases. Another such trend is seen at 14.9°. One large peak, consistent with the (10-2) reflection in the 25AMP/3-CH_3-BA cocrystal, gives way to a much smaller peak consistent with the (002) reflection of the 25AMP/3-Cl-BA cocrystal as the relative concentration of 3-CH_3-BA decreases. This transition is accompanied by a small peak consistent with the 25AMP/3-Cl-BA (111)

reflection at 15.5° growing from the baseline. Around 18° one peak migrates left slightly from top to bottom. This transition is actually the (021) reflection at 17.9° for **100% 0%** being replaced by the (11-2) reflection of **0% 100%** with increasing 25AMP/3-Cl-BA content from top to bottom. Should the crystals being analyzed contained both cocrystals rather than a solid solution of each, these peaks would exist simultaneously in each PXRD pattern rather than a clean transition from one to the other.

3.6.2.2. 25AMP:3-CH_3-BA:4-CH_3-BA

The 3-CH_3-BA/4-CH_3-BA series marks the successful creation of a multicomponent system containing components with substituents of different substitution positions. Although our previous studies have produced individual crystallizations containing both *meta*- and *para*-substituted moieties, this is the first system that was successfully crystallized and characterized across varying concentrations as a series.

FTIR data for the 3-CH_3/4-CH_3 series was also compiled and stacked for easy comparison. Figure 36 shows the collection of FTIR data with similar trending patterns denoted with arrows.

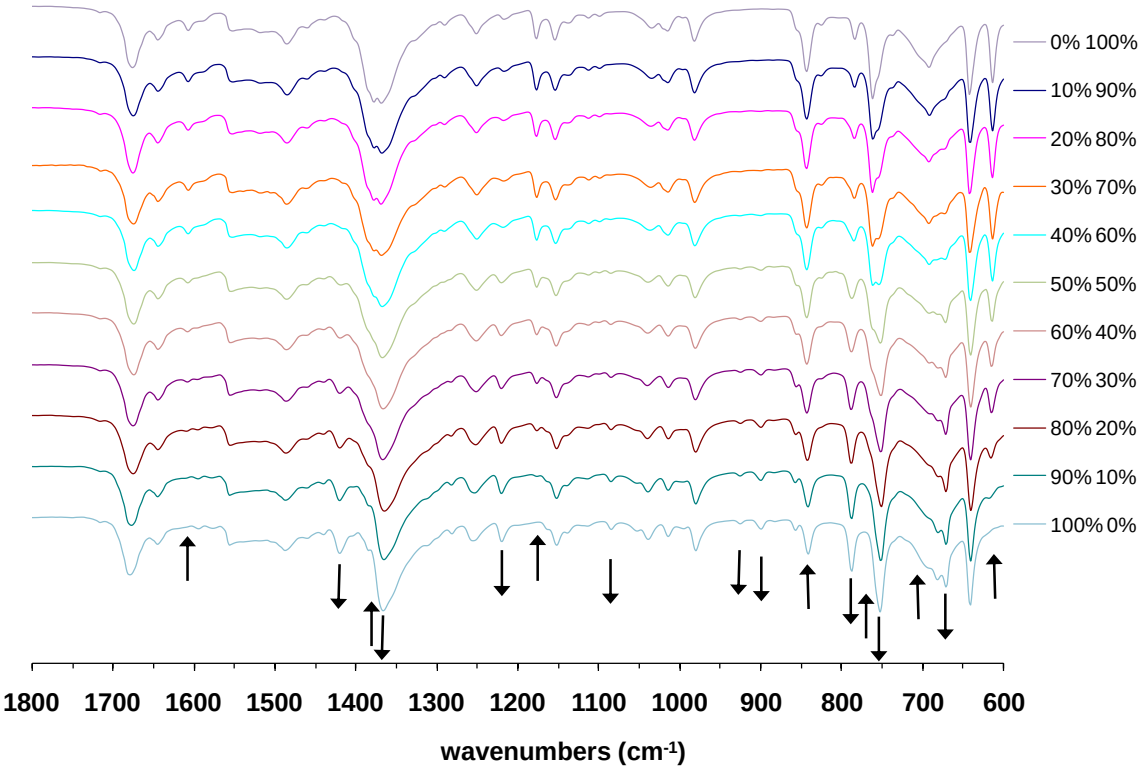

Figure 37. Stacked FTIR spectra for the 25AMP/3-CH_3-BA/4-CH_3-BA series. Each solid solution is labeled in the format X% Y%: the first number indicates the percent amount of 3-CH_3-BA and the second indicates percent 4-CH_3-BA. Arrows denote changes in peak intensity from top to bottom.

Intense dual peak transitions at 1377 cm^{-1}/1370 cm^{-1}, 761 cm^{-1}/752 cm^{-1} and single peak transitions seen at 786 cm^{-1} and 613 cm^{-1} highlight the most dramatic of trends for FTIR data of the 3-CH_3/4-CH_3 solid solution series. Starting as a broad band with two peaks in the **0% 100%** spectrum, the 1377 cm^{-1}/1370 cm^{-1} transition concludes with the 1377 cm^{-1} band receding. The peaks at 761 cm^{-1}/752 cm^{-1} begin with 752 as a shoulder to the 761 peak. However, as the relative 3-CH_3-BA concentration increased, the peak at 761 cm^{-1} shrank into the baseline of the spectrum.

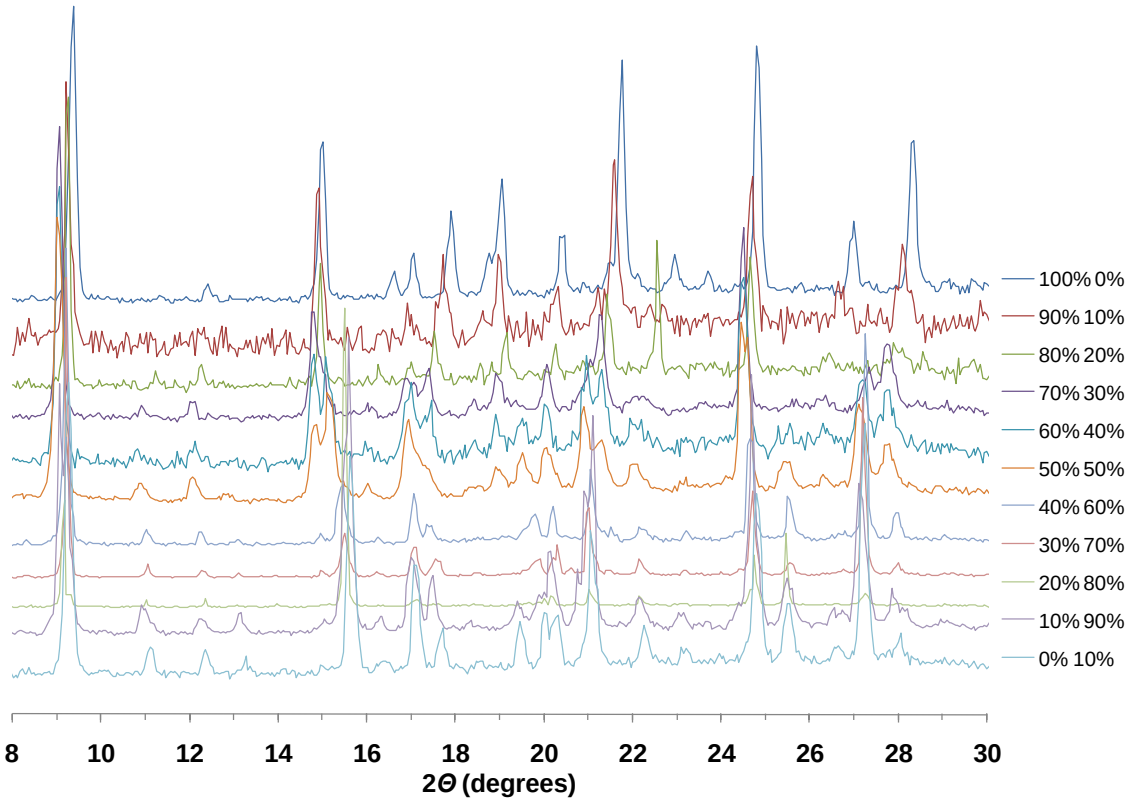

Figure 38. Stacked PXRD data for the 25AMP/3-CH_3-BA/4-CH_3-BA series. Each solid solution is labeled in the format X% Y%: the first number indicates the percent amount of 3-CH_3-BA and the second indicates percent 4-CH_3-BA.

With peak intensities and positions transitioning in the PXRD patterns we again have data reflecting a steady change in crystal contents (Figure 37). The peak at 9.3° shifts slight to the left from **100% 0%** to **0% 100%**. The two peaks in the respective cocrystals are both consistent with a (100) reflection, however, the 25AMP/3-CH_3-BA reflection is measured at 9.4° while the corresponding 25AMP/4-CH3-BA peak is located at 9.3°. Another transition is observed beginning with the peaks at 27.1° and 28.5°, consistent with (122) and (221) reflections within the **100% 0%** cocrystal. As observed from top to bottom, the two peaks slide closer to one another, while the left-hand peak grows and the right recedes. The peaks within the **0% 100%** dataset are found at 27.3° and 28.1° and correspond to (221) and (131) reflections, respectively.

3.7. Quaternary, Quinary, and Septary (Seven-Component) Solid Solutions

For the remaining crystalline products minimal data was collected. Unit cell data has been accumulated into tables for easy viewing where available. There is brief discussion of each tier of experiments.

Quaternary and quinary solid solution experiments characterized by single crystal X-ray diffraction continued to exhibit the same $P2_1/c$ space group while, in most cases, continuing to report unit cell volumes comparable to the mathematical averages of unit cell volumes for cocrystal combinations contained within the system. For values that deviate from the average, it is possible that the crystal selected may have included more or less of one acid than the other two. For example, the 25AMP/3-Cl-BA/3-Br-BA/3-I-BA product has a unit cell volume of 1267.064 $Å^3$. This is significantly less than the mathematical average of the 25AMP/3-Cl-BA, 25AMP/3-Br-BA, and 25AMP/3-I-BA cocrystal unit cell volumes ((1260.33 $Å^3$ + 1292.07 $Å^3$ + 1353.21 $Å^3$)/3 = 1301.87 $Å^3$). We speculate at this time that the crystal selected for analysis, although homogeneous, may have a crystallized without molar equivalents of benzoic acids, thus containing a greater relative concentration of 3-Cl-BA than the bromo- and iodobenzoic acids. Tables 13 and 14 contain unit cell data collected for the quaternary and quinary solid solution experiments.

Table 13. Structural data for quaternary solid solution experiments.

Compound	Space group	a [Å]	b [Å]	c [Å]	α [°]	β [°]	γ [°]	Volume [Å^3]
25AMP / 3-Cl-BA / 3-CH_3-BA / 3-Br-BA	-	-	-	-	-	-	-	-
25AMP / 3-Cl-BA / 3-CH_3-BA / 3-I-BA	$P2_1/c$	10.29	11.04	12.19	90	114.17	90	1263.404
25AMP / 3-Cl-BA / 3-Br-BA / 3-I-BA	$P2_1/c$	9.22	11.6	12.07	90	101.03	90	1267.064
25AMP / 3-CH_3-BA / 3-Br-BA / 3-I-BA	-	-	-	-	-	-	-	-
25AMP / 4-Cl-BA / 4-CH_3-BA / 4-Br-BA	$P2_1/c$	9.66	10.75	12.06	90	103.52	90	1217.665
25AMP / 4-Cl-BA / 4-CH_3-BA / 4-I-BA	$P2_1/c$	9.84	10.88	12.21	90	103.33	90	1281.718
25AMP / 4-Cl-BA / 4-Br-BA / 4-I-BA	$P2_1/c$	9.828	10.917	12.172	90	100.511	90	1284.028
25AMP / 4-CH_3-BA / 4-Br-BA / 4-I-BA	$P2_1/c$	9.815	10.904	12.198	90	101.911	90	1277.443

Note: Unit cell data was not collected for the 25AMP/3-Cl-BA/3-CH3-BA/3-Br-BA and 25AMP/3-CH3-BA/3-Br-BA/3-I-BA solid solutions.

Table 14. Structural data for quinary solid solution experiments.

Compound	Space group	a [Å]	b [Å]	c [Å]	α [°]	β [°]	γ [°]	Volume [Å^3]
25AMP / 3-Cl-BA / 3-CH_3-BA / 3-Br-BA / 3-I-BA	$P2_1/c$	10.25	11.05	12.2	90	113.71	90	1265.019
25AMP / 4-Cl-BA / 4-CH_3-BA / 4-Br-BA / 4-I-BA	$P2_1/c$	9.82	10.95	12.32	90	100.91	90	1300.813

Septary (seven-component) systems crystallized into large, brown crystals. Preliminary liquid chromatography-mass spectrometry analysis has shown molecular weights consistent with each of the seven crystallization components, but further method development and data analysis is necessary at this time.

4. Summary and Conclusions

Herein we have explained the design, creation, and identification of two, three, four, five, and seven component supramolecular solid solutions employing our 2-aminopyridine-benzoic acid supramolecular synthon. The synthon, well known in crystal engineering to date, has worked consistently throughout our studies without being influenced by changes in substituents or the number of materials crystallizing into a single crystal. Employing this supramolecular synthon, our studies have successfully crystallized systems with different substitutions on both the donor and acceptor moieties as well as products containing moieties with different substitution positions. Moreover, all of the products collected and characterized to date have identical packing structures, another first for any study we have previously performed. The products of these experiments have shown noticeable flexibility when including multiple components while exhibiting measurable variations in properties.

Characterization of crystalline products was completed by means of PXRD and SXRD, but also by DSC, and importantly FTIR. Both SXRD and PXRD are complex, timely, and expensive methods of analysis. Small outfits, start-ups and research groups may not have sufficient resources for such methods of analysis. We have shown how FTIR can be a very useful tool for determination of cocrystal and supramolecular solid solution crystal content by identifying obvious, visible trends in spectra. FTIR is an inexpensive, facile, and rapid method of characterization which until know has gone overlooked for characterizing continuous solid solutions.

Applications of supramolecular solid solutions to pharmaceutical drugs are being explored in our laboratories. With the modulation capabilities of solid solutions, crystalline products can be tailor-made to facilitate rapid dissolution and bioavailability in the body. But pharmaceuticals are not the only area of chemistry using supramolecular synthons. Solid state photochemical reactions are also employing cocrystals and solid

solutions. With cocrystals and supramolecular solid solutions of photoreactants locked into specific, regular geometries, photoreactions in the solid state have the ability of creating products with specificity not available in solution while also providing a green approach to synthesis.

Bibliography

[1] R. F. Tylecote, *A History of Metallurgy*, 2nd Ed., Inst. Of Materials, **1992.**

[2] J.-M. Lehn, *Supramolecular Chemistry*, **1995.**

[3] M. Cox, D. Nelson, *Lehninger Principles of Biochemistry*, 4th Ed., Palgrave Macmillan, **2004**.

[4] (a) C. J. Pedersen, *Angew. Chem. Int. Ed.*, **1998**, *27*, 1021.
(b) D. J. Cram, *Angew. Chem. Int. Ed.*, **1998**, *27*, 1009.
(c) J. -M. Lehn, *Angew. Chem. Int. Ed.*, **1998**, *27*, 89.

[5] *Comprehensive Supramolecular Chemistry*, Volume 1-11, Elsevier: New York.

[6] G. R. Desiraju, *Crystal Engineering: The Design of Organic Solids*, Elsevier: Amsterdam, **1989**.

[7] G. M. J. Schmidt, *Pure and Appl. Chem.*, **1971**, *27*, 647.

[8] G. R. Desiraju, *Angew. Chem. Int. Ed.* **1995**, 34, 2311.

[9] B. H. Meier, F. Graf, R. R. Ernst, *J. Chem. Phys.* **1981**, *76*, 767.

[10] P. Yakovchuk, E. Protozanova, M. D. Frank-Kamenetskii, *Nucleic Acids Res.*, **2006**, *34*, 564.

[11] J. A. Bis, M. J. Zaworotko, *Cryst. Growth Des.*, **2005**, *5*, 1169.

[12] G. R. Desiraju, *Cryst. Eng. Comm.*, **2003**, *5*, 466.

[13] J. D. Dunitz, *Cryst. Eng. Comm.*, **2003**, *5*, 506.

[14] A. D. Bond, *Cryst. Eng. Comm.*, **2007**, *9*, 833.

[15] G. P. Stahly, *Cryst. Growth. Des.* **2007**, *7*, 1007.

[16] A. I. Kitaigorodsky, *Mixed Crystals*. Springer-Verlag: New York, **1984**.

[17] M. C. Etter, *Acc. Chem. Res.* **1990**, *23*, 120.

[18] C. B. Aackeroy, M. E. Fasulo, J. Desper, *Mol. Pharm.*, **2007,** *4*, 317.

[19] S. L. Childs, G. P. Stahly, A. Park. *Mol. Pharm*. **2007**, *4*, 323.

[20] S. L. Johnson, K. A Rumon *J. Phys. Chem*., **1965**, *69*, 74.

[21] J. Berstein, *Polymorphism in Molecular Crystals*, Clarenden Press: Oxford, **2002.**

[22] H. G. Brittain, *Polymorphism in Pharmaceutical Solids*. Marcel Dekker: New York, **1999.**

[23] R. Hilfiker, *Polymorphism in the Pharmaceutical Industry*. Wiley-VCH: Weinheim, **2006**.

[24] N. J. Babu, L. S. Reddy, S. Aitipamula, A. Nangia, *Chem. Asian J.*, **2008**, *3*, 1122.

[25] M. L. Brader, M. Sukumar, A. H. Pekar, D. S. McClellan, R. E. Chance, D. B. Flora, A. L. Cox, L. Irwin, S. R. Myers, *Nature Biotechnology*, **2002**, *20*, 800.

[26] M. Dabros, P.R. Emery, V.R. Thalladi, *Angew. Chem. Int. Ed.*, **2007**, *46*, 4132.

[27] US Food and Drug Administration/Center for Food Safety and Applied Nutrition, Food Additive Status List, revised July 2006. http://www.cfsan.fda.gov/~acrobat/opa-appa.pdf.

[28] D. Boenigk, D. Mootz, *J. Am. Chem. Soc.*, **1988,** *110*, 2135.

[29] J. A. Cowan, J. A. K. Howard, G. J. McIntyre, S. M.-F. Lo, I. D. Williams, *Acta. Cryst.*, **2003**, *B59*, 794.

[30] Bond angles are measured from refcode AMMEPY in the Cambridge Structural Database.

[31] Bond angles are measure from refcode AMPYRC in the Cambridge Structural Database.